OUKA
The University of Osaka
Institutional Knowledge Archive

Title	Laser-induced Carbonization of Sumanene Derivatives
Author(s)	稲田, 雄飛
Citation	大阪大学, 2015, 博士論文
Version Type	VoR
URL	https://doi.org/10.18910/52128
rights	
Note	

The University of Osaka Institutional Knowledge Archive : OUKA

https://ir.library.osaka-u.ac.jp/

The University of Osaka

Doctoral Dissertation

Laser-induced Carbonization of Sumanene Derivatives

（スマネン誘導体のレーザ誘起炭素化）

Yuhi Inada

January 2015

Department of Applied Chemistry

Graduate School of Engineering

Osaka University

Preface

The studies presented in this thesis were carried out under the guidance of Professor Toshikazu Hirao, Department of Applied Chemistry, Graduate School of Engineering, Osaka University during 2010-2015.

The objects of this dissertation are studies on laser-induced carbonization of sumanene derivatives and structural and catalytic characterization of the products.

The author hopes that this fundamental work described in this thesis contributes toward further development of applications using graphitic-carbon-based materials such as drawing of conductive pattern and electrocatalysts in a fuel cell.

Yuhi Inada

Department of Applied Chemistry
Graduate School of Engineering
Osaka University
Suita, Osaka
Japan

January, 2015

Contents

General Introduction		1
Chapter 1.	Dependence of Conductivity on Laser Annealing Energy and Time in Laser-induced Carbonization of Sumanene Derivatives	13
Chapter 2.	Structural and Catalytic Properties of the Carbonized Product through Laser Annealing of Sumanene Derivatives	23
Chapter 3.	Energy Threshold of Laser-induced Carbonization in Sumanene Derivatives	37
Conclusion		67
List of Publications		68
List of Supplementary Publications		69
Acknowledgement		70

General Introduction

i−1. Background

Carbonous compounds including graphitic lattice,[1] which consist of fused benzene rings, have been actively studied due to the wide applicability toward conducting and catalytic materials.[2] Among the methods to synthesize such carbonous compounds, laser-induced carbonization of organic compounds[3] (Figure i−1a) has been expected as one of the useful methods toward electronic device application owing to the advantages such as rapid heating[4] and high-resolution patterning (Figure i−1b). Here, laser is abbreviation of light amplification by stimulated emission of radiation. Laser device gives highly directional light where the wavelength, phase difference, and polarization are constant. While the laser device invented for the first time emits continuous microwave,[5] pulse oscillation laser devices in the ultraviolet light appeared in the 1980's, which gave instantaneous higher-output power than continuous-wave (CW) laser. Taking this opportunity, pulse-laser irradiation toward polymers have been studied. Raffel et al. reported the increase of electrical conductivity of a polyimide film induced by argon ion pulse laser in 1983 to repair circuit wiring.[3a] This appears to be the first

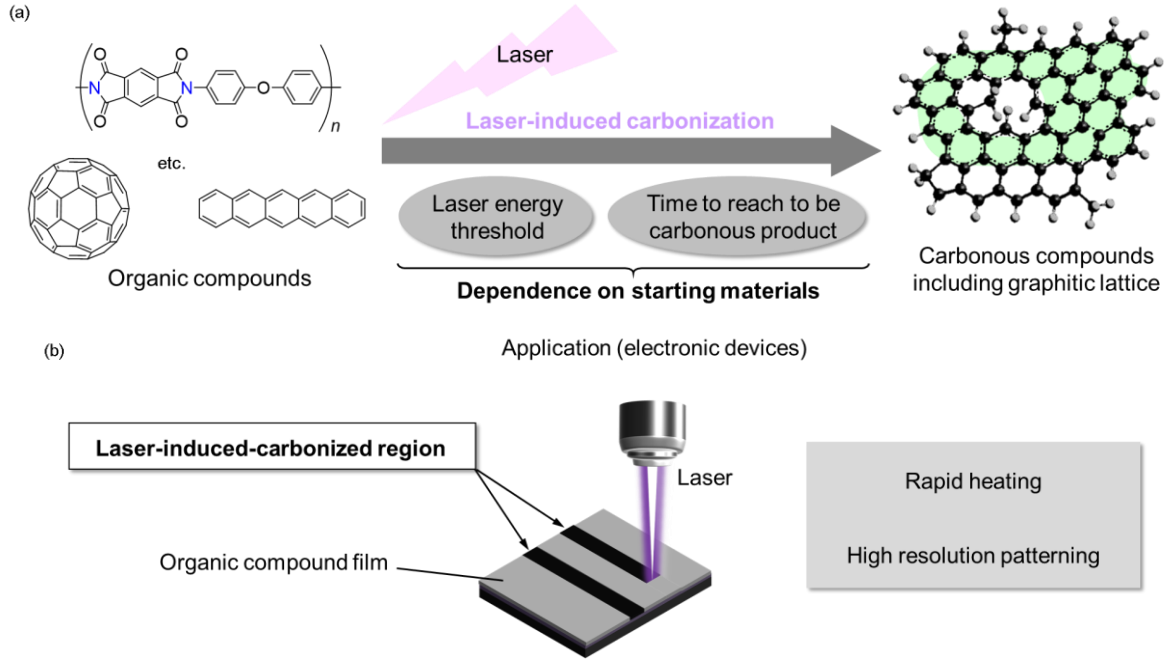

Figure i−1. (a) Laser-induced carbonization of organic compounds and (b) its applications.

example of laser-induced carbonization. Subsequently, many researchers reported the laser-induced carbonization employing various polymers and low molecular weight compounds as starting materials as follows.

Starting Materials for Laser-induced Carbonization

Polymers

Polyimide (Kapton®) film is a starting material often-used in the laser-induced carbonization, where the wavelength of the pulse lasers was 248 nm,[3c, 6] 308 nm,[7] and 1064 nm.[8] The pulse-laser-induced carbonization of the following halogenated polyethylenes were also reported: chlorinated polyvinyl chloride [(CHCl−CHCl)$_n$], that is known as a highly photosensitive polymer[3b] and ethylene-tetrafluoroethylene copolymers [(CH$_2$−CH$_2$)$_n$(CF$_2$−CF$_2$)$_m$, 248 nm],[3d] [(CH$_2$−CH$_2$−CF$_2$−CF$_2$)$_n$, 193, 248, and 308 nm],[9] and [(CH$_2$−CF$_2$)$_n$, 248 nm].[10] Films of polybenzimidazole (PBI, 248 nm),[3c] polyacrylonitrile (PAN, CO_2 laser),[11] and a positive photoresist (OiR897-101, Olin Corp., Norwalk, CT) that consists of predominantly novolak resins (514 and 632 nm CW laser)[3i] were also included as such an example.

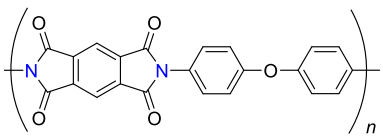

Polyimide (Kapton®)

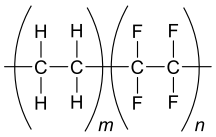

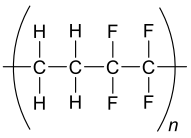

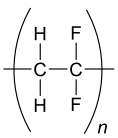

Ethylene-tetrafluoroethylene copolymers

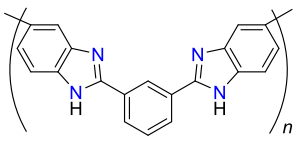

Polybenzimidazole (PBI)

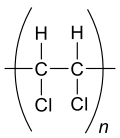

Chlorinated polyvinyl chloride

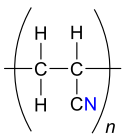

Polyacrylonitrile (PAN)

Low molecular weight compounds

Solid of fullerene C_{60} was also a starting material that was often studied on the laser-induced carbonization, where 248,[3e] 308,[3h] 355,[3j] and 1064 nm[3g] pulse lasers were employed. Other such examples includes

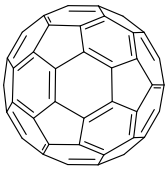

Fullerene C_{60}

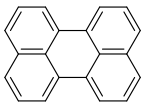

Perylene

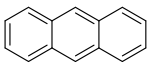

Anthracene

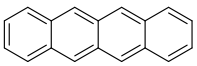

Tetracene

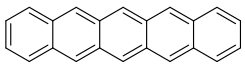

Pentacene

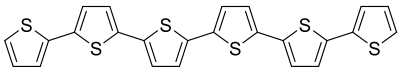

Sexithiophene (6T)

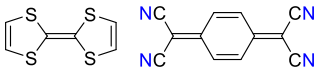

(TTF)(TCNQ)
TTF: tetrathiafulvalene
TCNQ:tetracyanoquinodimethane

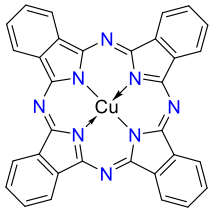

Copper phthalocyanine (CuPc)

aromatic hydrocarbons such as perylene, anthracene, tetracene (7.6 μm pulse laser),[12] and pentacene (355 nm pulse laser),[3j] and aromatic hydrocarbons that consists of hetero atoms[3j] such as sexithiophene (6T), (TTF)(TCNQ) [TTF: tetrathiafulvalene; TCNQ:tetracyanoquinodimethane], and copper phthalocyanine (CuPc). Also, the behavior of laser-induced carbonization is considered to be significantly affected by factors such as wavelength, energy, and pulse duration of laser employed.

In laser-induced carbonization of a starting material, as the laser energy per unit area is increased, it is gradually decomposed, and then carbonized in excess of a laser energy threshold. Because it is difficult to strictly examine the threshold, here simply describing “threshold”, it shall indicate a threshold range possessing a certain width from this point forward. Near the threshold energy (above the threshold), the more laser energy is supplied, the more rapidly the starting material is carbonized. Laser irradiation with further more energy induces laser ablation, which involves explosive erosion.

Such energy threshold of laser-induced carbonization and time to reach carbonous product are important factors influencing the efficiency of carbonization. Therefore, comparison of these factors among starting materials leads to the dependence on starting materials (Figure i−1a). The starting materials having the lower threshold and shorter time to reach carbonous product are considered to be useful in laser-induced carbonization. There is no reports to study laser-induced carbonization from such a viewpoint to the best of my knowledge.

Synthetic Methods of NGC

NGCs are known to be promising materials as a cathode catalyst of fuel cells due to the high activity toward oxygen reduction reaction (ORR).[13] Synthetic methods of NGC includes thermal pyrolysis of nitrogen-containing compounds such as low molecular weight compounds, ionic liquid, and polymers in a solid or liquid state, laser pyrolysis of nitrogen-containing polymers, and other methods as follows.

Thermal Pyrolysis of Nitrogen-containing Compounds

1. Low Molecular Weight Nitrogen-containing Aromatic Compounds

This classification consists of nitrogen-containing aromatic compounds. Pyrazine (PZ), pyridine (PR), quinoline (QN), and phenazine (PN) were pyrolyzed at 800, 1000, 1200, and 1600 °C under the pressure of ~300 mmHg.[14] As the temperature increased, the nitrogen contents decreased. For PZ, PR, and QN, the remaining proportions of nitrogen atoms at 1200 °C were only 5−7%, while those at 800 °C were 15−39%. In the case of PN, 53% nitrogen atoms remained at 800 °C, while 15% at 1200 °C.

Other starting materials include carbazole and acridine, where the ratio of nitrogen atoms toward carbon atoms (N/C ratio) fell to 22% and 53% at 1000 °C in argon for 1 h, respectively.[15] Thus, durability toward the elimination of nitrogen atoms largely depends on a starting material.

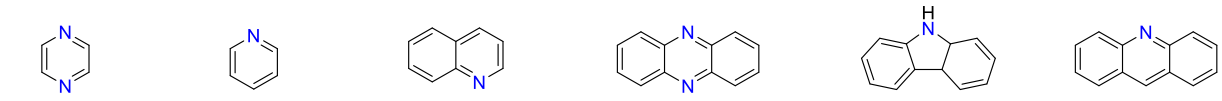

2. Ionic Liquids

As the examples of pyrolytic synthesis of ionic liquids, EMIM-dca and 3-MBP-dca were reported [1-ethyl-3-methylimidazolium (EMIM), 3-methyl-1-butylpyridine (3-MBP), dicyanamide (dca)].[16] While the nitrogen content of EMIM-dca decreased from ~40 wt% (400 °C, 1 h) to ~10 wt% (1000 °C, 1 h), that of 3-MBP-dca decreased from ~29 wt% (400 °C, 1 h) to ~9 wt% (1000 °C, 1 h).

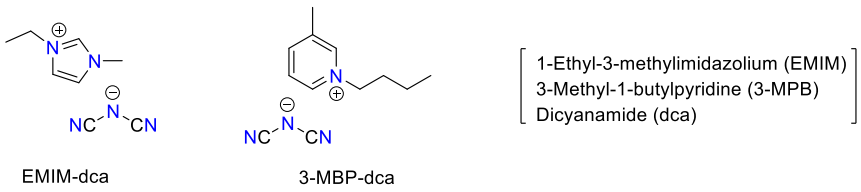

3. Polymers

First part describes the polymers that include nitrogen atoms in the ring structure. Among the pyrolytic synthetic methods of NGCs, the report on a polyimide (Kapton®) film by Bruck appears to be first example, revealing that the Kapton® film showed the high durability toward the elimination of nitrogen atoms at 800 °C for 1 h under the pressure of ~5 × 10^{-6}, where 89% nitrogen atoms remained.[17] In contrast, only 27% nitrogen atoms were left in the residue resulted from the pyrolysis up to 1000 °C (30 K h^{-1}) in nitrogen.[18] Pyrolysis of another polyimide (Pyralin®, chemical structure was not disclosed) film was also reported. When the film was heated at 200 °C for 2 h in air, 63% nitrogen atoms remained. Then, the pyrolyzed sample was furthermore treated at 700 °C for 4 h in argon to leave 50% nitrogen atoms.[19]

As a starting material for carbonization, poly(*p*-phenylene-1,3,4-oxadiazole) (POD) was reported by Murakami et al..[20] The N/C ratio severely decreased to 18% of that before heating at 1000 °C in argon. In contrast, pyrolysis of polyquinoline (PQ) film in a vacuum sealed tube was conducted by Chiang et al. to give the important information as below: while the N/C ratio was retained at 600 °C, that reduced to 90% of original one at 700 °C and saturated at half amount at the temperature between 800 and 1200 °C.[21]

Piao et al. reported the pyrolysis of the ladder polymer named PMDA-DAB prepared through polycondensation of pyromellitic dianhydride (PMDA) and 3,3'-diaminobenzidine (DAB).[22] The N/C ratio fell down to 64 and 18% of that of pristine sample by heating in nitrogen at 800 and 1200 °C, respectively. In contrast, in the case of step-ladder polymer named DEDA-TADPE obtained by polycondensation of diphenylether dianhydride (DEDA) and tetraamino diphenylether (TADPE), its pyrolysis in nitrogen at 800 and 1200 °C made the N/C ratio reduce to 42 and 0% of that of the raw sample.[23] Therefore, it is intriguing that the decrease rate of the N/C ratio differs between these two starting materials even though the environment of nitrogen atoms are similar due to possessing the same partial structure.

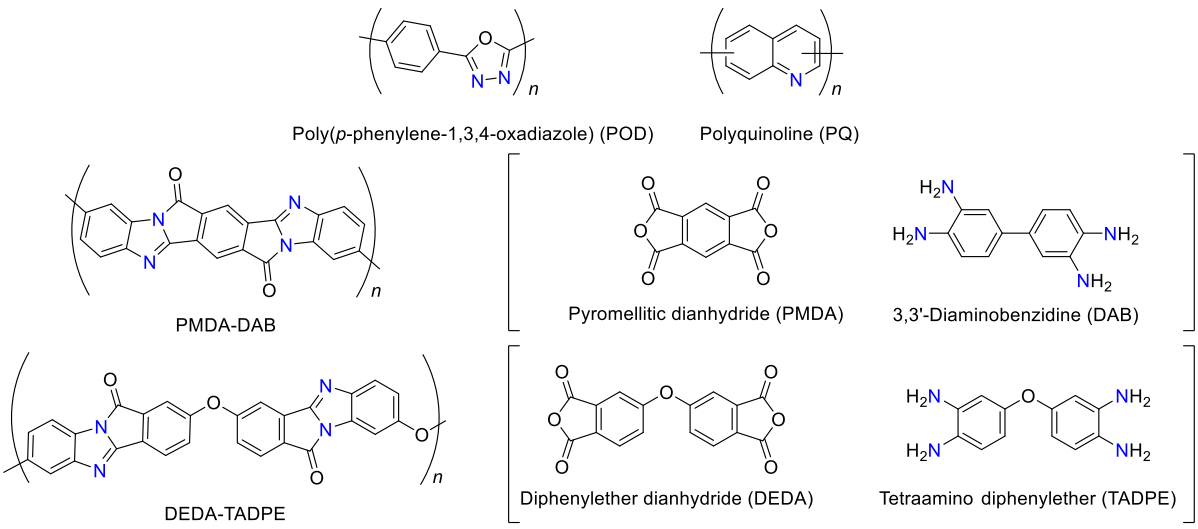

Next part describes the polymers that do not include nitrogen atoms in the ring structure. PAN is such a stating material. When PAN was heated up to 300, 500, and 800 °C (1 K min^{-1}) and soaked for 1 h in argon, the N/C ratio fell to 61, 59, and 39%, respectively.[15]

Laser Pyrolysis of Nitrogen-containing Polymers

There are a few reports on laser pyrolysis of nitrogen-containing compounds, where a polyimide (Kapton®) film was employed as a starting material. In the report on the irradiation using a 248 nm pulse laser, nitrogen atoms were observed by XPS (see 2−2−3 of Chapter 2 in detail about the general instruction) below the laser energy of 5.6 J cm^{-2}, while they were not observed above the laser energy of 56 J cm^{-2}.[6a] It was reported that a 308 nm laser at the energy of 225 mJ cm^{-2} decreased the content of nitrogen atoms, which was confirmed by XPS.[7] The irradiation of 1064 nm pulse laser at 632 mJ cm^{-2} (per pulse) implied existence of nitrogen atoms through Raman spectroscopy (see 2−2−1 of Chapter 2 in detail about the general instruction).[24]

Other methods

Because I did not focus on graphene (mono or a few-layer graphite) in this thesis, the methods to synthesize nitrogen-doped graphene are briefly described as follow: 1) solvothermal synthesis with heating a mixture of sodium and ethanol[25] or a mixture of carbon tetrachloride and lithium nitride[26] in a sealed reactor vessel, 2) chemical vapor deposition (CVD) from gas mixtures containing carbon and nitrogen source[27] or liquid organic

precursors such as acetonitrile or pyridine,[28] 3) segregation growth utilizing a nickel/boron bilayer including carbon and nitrogen source,[29] 4) arc discharge using graphite electrodes in the vapor of nitrogen-containing compounds such as pyridine or ammonia,[30] and 5) nitrogen doping to graphite through laser heating in the presence of pyrrole or 3-methylthiophene vapors.[31]

i−2. Objective of the thesis

A bowl-shaped molecule sumanene ($C_{21}H_{12}$, **1**, Figure i−2a), a partial structure of fullerene C_{60}, was synthesized for the first time[32] and strenuously studied to reveal its properties in the author's laboratory.[33] It is considered to be interesting from viewpoints of not only academic study but also materials application to uncover properties derived from the bowl-shaped structure and the strain of sumanene. For example, it was discovered in the author's laboratory that bowl-shaped sumanene molecules assemble to form a column-likepacking structure in a solid state, exhibiting charge carrier mobility comparable to that of fullerene C_{60} (0.75 $cm^2 V^{-1}s^{-1}$) in the assembly direction through below-mentioned time-resolved microwave conductivity (TRMC) method[34] (Chapter 1, 1−2−1). More strained bowl was also reported to be synthesized from sumanene.[35]

Moreover, sumanenes combined with aniline derivatives **2** and **3** were synthesized. Their conductivities were evaluated through TRMC method[36] (Figure i−2b). In the measurement, 355 nm nanosecond pulsed laser was employed as an exciting source. After the laser irradiation to the samples at a higher power than that at the

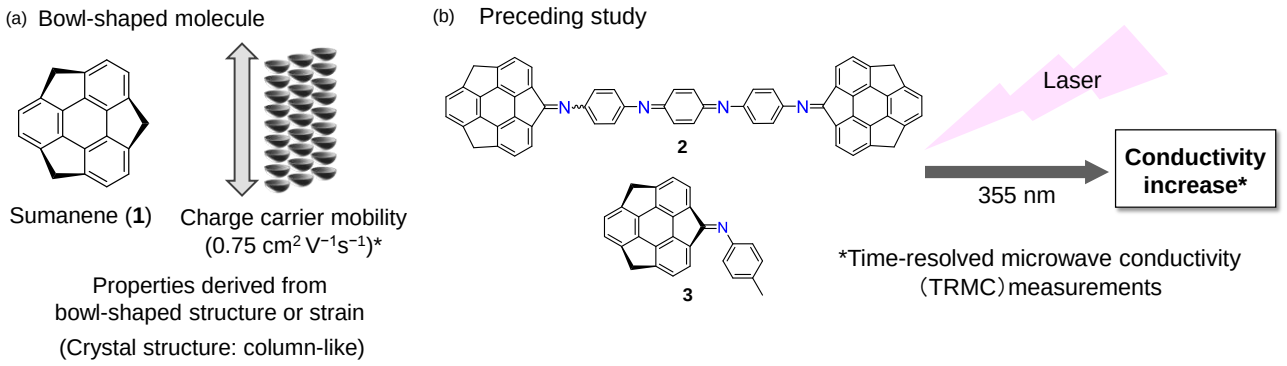

Figure i−2. (a) Bowl-shaped molecule, sumanene (**1**) and schematic illustration of its packing structure in the crystal state with the carrier mobility in the stacking direction. (b) Preceding study: conductivity increase induced through laser irradiation to sumanene imine derivatives **2** and **3**.

TRMC measurements, their conductivities were drastically increased.[36] Due to the interesting discovery, this study started. From the later literature survey, it was turned out that such phenomena have been reported with the other compounds such as fullerene C_{60},[3e, 3g, 3h, 3j] polymers including polyimide,[3a-d, 3f, 3i] and π-conjugated molecules[3j] (Figure i−1a) as described above. However, there have been no such reports in any bowl-shaped molecules.

In this context, laser-induced carbonization of sumanene derivatives **2**−**6** synthesized through benzylic oxidation of sumanene or imination of the oxosumanene were studied in addition to sumanene (**1**) itself (Figure i−3) because environment around strained benzyl carbons of sumanene is expected to affect the laser-induced carbonization. Usage of nitrogen-containing molecules such as **2**, **3**, **6** will lead to the synthesis of nitrogen-doped graphitic carbons (NGCs) through laser-induced carbonization.

Laser-induced carbonization of sumanene derivatives was studied in this thesis from the four views as below: 1) following reactions involving laser-induced carbonization, 2) structural and electrical properties of products obtained from laser-induced carbonization, 3) catalytic properties of NGC synthesized through laser-induced carbonization, and 4) energy threshold of laser-induced carbonization (Figure i−3).

The significance of this study lies in 1) comparing the behavior of laser-induced carbonization of sumanene having strained bowl-shaped skeleton with that of other π-conjugated small molecules having similar chemical structures of sumanene, and 2) revealing the applicability of thus-synthesized carbonous products as conducting

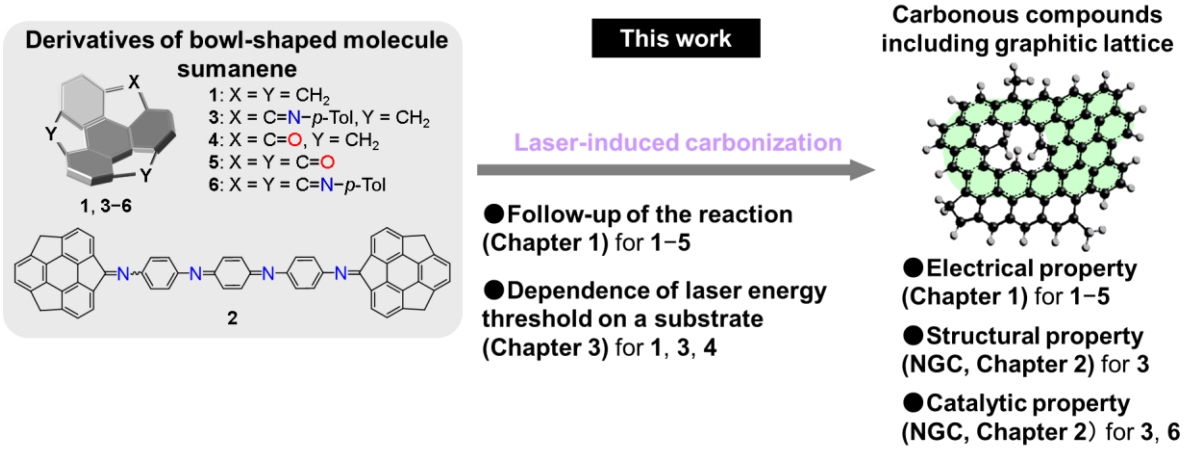

Figure i−3. This work: laser-induced carbonization of derivatives of bowl-shaped molecule sumanene.

and catalytic materials.

i−3. Outline of the thesis

This thesis describes dependence of the behavior of laser-induced carbonization of sumanene derivatives, and structural and catalytic properties of the carbonous products. Chapter 1 explores dependence of conductivity on laser annealing energy and time in laser-induced carbonization of sumanene derivatives. Chapter 2 reports structural and catalytic properties of the carbonized products through laser annealing of sumanene derivatives. Chapter 3 focuses on energy threshold of laser-induced carbonization of sumanene derivatives.

References and Notes

[1] Generally graphitic carbons are associated with carbons having laminated structure and high crystallinity. In this thesis, graphitic carbons indicate the compounds mainly including sp^2-bonded clusters consisting of fused benzene nuclei. The graphitic carbons show electrical conductivity in contrast to diamond-like carbons with a lot of sp^3-bonded carbons.

[2] a) D. D. L. Chung, *J. Mater. Sci.* **2004**, *39*, 2645-2661; b) E. Antolini, *Appl. Catal., B* **2012**, *123-124*, 52-68.

[3] a) J. I. Raffel, J. F. Freidin, G. H. Chapman, *Appl. Phys. Lett.* **1983**, *42*, 705-706; b) C. Decker, *J. Polym. Sci., Part C: Polym. Lett.* **1987**, *25*, 5-10; c) M. Schumann, R. Sauerbrey, M. C. Smayling, *Appl. Phys. Lett.* **1991**, *58*, 428-430; d) S. Kawanishi, Y. Shimizu, S. Sugimoto, N. Suzuki, *Polymer* **1991**, *32*, 979-983; e) H. M. Phillips, D. Sarkar, N. J. Halas, R. H. Hauge, R. Sauerbrey, *Appl. Phys. A: Solids Surf.* **1993**, *57*, 105-107; f) R. Srinivasan, R. R. Hall, D. C. Allbee, *Appl. Phys. Lett.* **1993**, *63*, 3382-3383; g) M. Ferretti, A. Parisini, M. Manfredini, P. Milani, *Chem. Phys. Lett.* **1996**, *259*, 432-437; h) D. Ning, Q. H. Lou, J. X. Dong, Y. R. Wei, *Appl. Phys. A* **1996**, *62*, 509-512; i) R. Kostecki, X. Song, K. Kinoshita, *Electrochem. Solid-State Lett.* **2002**, *5*, E29-E31; j) J. I. Inoue, H. Wada, T. Mori, *Jpn. J. Appl. Phys.* **2010**, *49*, 0716051-0716055.

[4] Z. Y. Qin, B. Y. Du, J. Zhang, T. B. He, L. Qin, Y. S. Zhang, *Appl. Phys. A* **2001**, *72*, 711-715.

[5] A. L. Schawlow, C. H. Townes, *Physical Review* **1958**, *112*, 1940-1949.

[6] a) H. Tsubakihara, M. Takeda, K. Okada, A. Sakamoto, *Kobunshi Ronbunshu* **1994**, *51*, 361-363; b) Z. Qin, X. Huang, D. Wang, T. He, Q. Wang, Y. Zhang, *Surf. Interface Anal.* **2000**, *29*, 514-518.

[7] T. Lippert, E. Ortelli, J. C. Panitz, F. Raimondi, J. Wambach, J. Wei, A. Wokaun, *Appl. Phys. A* **1999**, *69*, S651-S654.

[8] M. Endo, N. Kota, S. Ishibe, M. Ueda, K. Oshida, T. Kasai, *T. IEE Japan* **1997**, *117*, 638-644.

[9] Y. Hamada, S. Kawanishi, M. Nishii, S. i. Sugimoto, T. Yamamoto, *Jpn. J. Appl. Phys., Part 1* **1994**, *33*, 4764-4768.

[10] Y. Ji, Y. Jiang, *Appl. Phys. Lett.* **2006**, *89*, 221103.

[11] T. Saito, T. Kawaguchi, I. Satoh, in *ASME/JSME 2011 8th Thermal Engineering Joint Conference, AJTEC 2011, Vol. 2011*, **2011**.

[12] K. Tono, H. Kondoh, Y. Hamada, T. Suzuki, K. Bito, T. Ohta, S. Sato, H. O. Hamaguchi, A. Iwata, H. Kuroda, *Jpn. J. Appl. Phys., Part 1* **2005**, *44*, 7561-7567.

[13] X. Zhou, J. Qiao, L. Yang, J. Zhang, *Adv. Energy Mater.* **2014**, *4*, 1301523.

[14] D. P. Kim, C. L. Lin, T. Mihalisin, P. Heiney, M. M. Labes, *Chem. Mater.* **1991**, *3*, 686-692.

[15] J. R. Pels, F. Kapteijn, J. A. Moulijn, Q. Zhu, K. M. Thomas, *Carbon* **1995**, *33*, 1641-1653.

[16] B. J. P. Paraknowitsch, J. Zhang, D. Su, A. Thomas, M. Antonietti, *Adv. Mater.* **2010**, *22*, 87-92.

[17] S. D. Bruck, *Polymer* **1965**, *6*, 319-332.

[18] A. Bürger, E. Fitzer, M. Heym, B. Terwiesch, *Carbon* **1975**, *13*, 149-157.

[19] J. I. Gittleman, E. K. Sichel, *J. Electron. Mater.* **1981**, *10*, 327-336.

[20] M. Murakami, H. Yasujima, Y. Yumoto, S. Mizogami, S. Yoshimura, *Solid State Commun.* **1983**, *45*, 1085-1088.

[21] L. Y. Chiang, J. P. Stokes, D. C. Johnston, D. P. Goshorn, *Synth. Met.* **1989**, *29*, 483-488.

[22] M. Piao, M. Wan, F. Lu, *J. Polym. Sci., Part A: Polym. Chem.* **1996**, *34*, 1567-1572.

[23] M. Piao, M. Wan, F. Lu, *Synth. Met.* **1997**, *89*, 209-213.

[24] M. Endo, K. Hakamada, C. Kim, N. Miyazawa, T. Kasai, *Tanso* **1998**, *183*, 156-161.

[25] M. Choucair, P. Thordarson, J. A. Stride, *Nat. Nanotechnol.* **2009**, *4*, 30-33.

[26] D. Deng, X. Pan, L. Yu, Y. Cui, Y. Jiang, J. Qi, W. X. Li, Q. Fu, X. Ma, Q. Xue, G. Sun, X. Bao, *Chem. Mater.* **2011**, *23*, 1188-1193.

[27] a) D. Wei, Y. Liu, Y. Wang, H. Zhang, L. Huang, G. Yu, *Nano Lett.* **2009**, *9*, 1752-1758; b) Z. Luo, S. Lim, Z. Tian, J. Shang, L. Lai, B. MacDonald, C. Fu, Z. Shen, T. Yu, J. Lin, *J. Mater. Chem.* **2011**, *21*, 8038-8044; c) L. Qu, Y. Liu, J. B. Baek, L. Dai, *ACS Nano* **2010**, *4*, 1321-1326.

[28] a) A. L. M. Reddy, A. Srivastava, S. R. Gowda, H. Gullapalli, M. Dubey, P. M. Ajayan, *ACS Nano* **2010**, *4*, 6337-6342; b) Z. Jin, J. Yao, C. Kittrell, J. M. Tour, *ACS Nano* **2011**, *5*, 4112-4117.

[29] C. Zhang, L. Fu, N. Liu, M. Liu, Y. Wang, Z. Liu, *Adv. Mater.* **2011**, *23*, 1020-1024.

[30] L. S. Panchakarla, K. S. Subrahmanyam, S. K. Saha, A. Govindaraj, H. R. Krishnamurthy, U. V. Waghmare, C. N. R. Rao, *Adv. Mater.* **2009**, *21*, 4726-4730.

[31] C. A. Kuper, M. M. Labes, *Chem. Mater.* **1999**, *11*, 408-411.

[32] H. Sakurai, T. Daiko, T. Hirao, *Science* **2003**, *301*, 1878.

[33] T. Amaya, T. Hirao, *Chem. Commun.* **2011**, *47*, 10524-10535.

[34] T. Amaya, S. Seki, T. Moriuchi, K. Nakamoto, T. Nakata, H. Sakane, A. Saeki, S. Tagawa, T. Hirao, *J. Am. Chem. Soc.* **2009**, *131*, 408-409.

[35] H. Sakurai, T. Daiko, H. Sakane, T. Amaya, T. Hirao, *J. Am. Chem. Soc.* **2005**, *127*, 11580-11581.

[36] Y. Shimizu, *Master thesis* **2010**.

Chapter 1. Dependence of Conductivity on Laser Annealing Energy and Time in Laser-induced Carbonization of Sumanene Derivatives [1,2,3]

1−1. Introduction

Laser-induced carbonization of organic compounds[1] has been expected as one of the important ways toward electronic device application due to the merits such as rapid heating[2] and high-resolution patterning. In fact, some examples have been reported as follows: drawing of conducting pattern onto a film of organic compounds[1a, 1f, 1i] and organic transistors where the carbonized surface is utilized as electrodes.[1j] Usefulness of such electrodes has been attracting much interests because they show better affinity to organic materials than metal electrodes. [1j] Although the carbonous electrodes employed here possess structural defects, they work well as electrodes. Following the conductivity change of a substrate during laser irradiation allows us not only to evaluate the conductivity but also to monitor the progress of the carbonization reaction.

In this chapter, the reactions involving laser-induced carbonization were followed using conductivity as a probe in order to examine the laser irradiation conditions where laser-induced carbonization can occur in sumanene derivatives. TRMC method (see the details in this chapter, 1−2−1) was utilized for this aim because this method can sensitively detect the change of conductivity in nanometer scale. Moreover, to study applicability toward conducting materials, the electrical conductivity in submillimeter scale was measured using direct-current (DC) method (see the details in this chapter, 1−2−2).

1−2. Results and Discussion

1−2−1. Dependence of Time-resolved Microwave Conductivity on Laser Annealing Energy and Time in Laser-induced Carbonization of Sumanene Derivatives[1,2,3]

In this chapter, the conductivity of sumanene derivatives during laser irradiation was followed through the TRMC method. In this method, the nanometer-scale mobility of the charge carriers generated by laser pulse irradiation is quantified using oscillating microwaves without electrodes. [3] The data obtained here are a

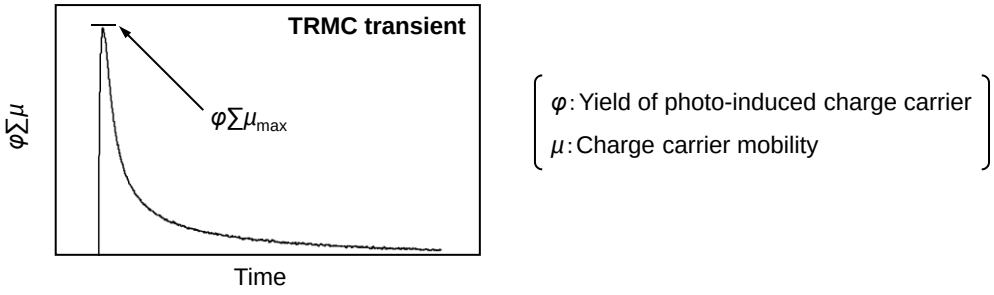

Figure 1−1. Schematic diagram of TRMC transient decay profile. $\varphi\sum\mu_{max}$ indicates the maximum value of $\varphi\sum\mu$.

transient signal of $\varphi\sum\mu$ (φ: generation yield of photo-induced charge carriers, $\sum\mu$: sum of the mobilities for the positive and negative charge carriers). The maximum value of $\varphi\sum\mu$ shall be expressed as $\varphi\sum\mu_{max}$ (Figure 1−1). Laser irradiation in order to change the conductivity of a sample shall be described as laser annealing. In this chapter, a Nd:yttrium aluminum garnet (Nd:YAG) laser (wavelength: 355 nm, pulse duration: 5−8 ns, pulse repetition rate: 10 Hz) was employed not only for laser annealing of a sample but also for the TRMC measurements as an excitation source under ambient pressure and atmosphere (Figure 1−2a). The laser

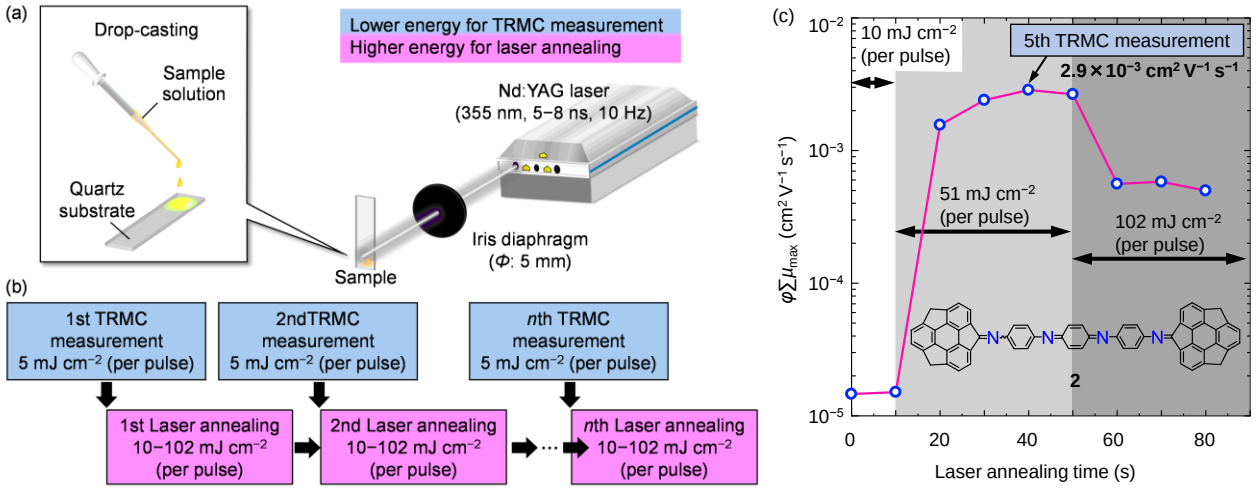

Figure 1−2. (a) Schematic illustration for laser annealing, where TRMC measurements were inserted to monitor the conductivity change. The balloon exhibits preparation of sample films drop-casted from a CH_2Cl_2 solution of **2** or **3**. (b) Experimental sequence to investigate laser annealing time dependence of conductivity for **2** and **3**. (c) Laser annealing time dependence of $\varphi\sum\mu_{max}$ for the laser-annealed film of **2**. Each TRMC was measured under excitation at 355 nm and 5 mJ cm^{-2} (per pulse). White, gray, and dark gray tracks represent the laser energy for laser annealing: 10, 51, and 102 mJcm^{-2} (per pulse), respectively.

parameter employed was selected so as to agree with that of previous report.[4] To monitor the conductivity change of the sample during laser annealing, TRMC measurements were inserted with every laser annealing for several seconds (Figure 1−2b). During the TRMC measurements, the laser energy was decreased down to 5 mJ cm^{-2} (per pulse) to avoid the conductivity change due to the degradation of the sample.

The study began with the closer investigation of compound **2**, which showed the dramatic increase of the conductivity by laser annealing as mentioned in the introduction. First, to grasp the energy range for laser annealing where the conductivity can be increased, dependence of $\varphi\sum\mu_{max}$ for **2** on both energy and time for laser annealing was examined (Figure 1−2c). The laser energy was stepwise increased [10, 51, 102 mJ cm^{-2} (per pulse)], where 102 mJ cm^{-2} (per pulse) was maximum output of the laser employed. The value of $\varphi\sum\mu_{max}$ before laser annealing was on the order of typical semiconductor (1.5×10^{-5} cm^2 V^{-1} s^{-1}). Although the laser annealing at the energy of 10 mJ cm^{-2} (per pulse) could not make obvious changes in $\varphi\sum\mu_{max}$, that at 51 mJ cm^{-2} (per pulse) abruptly increased the $\varphi\sum\mu_{max}$ to record the local maximum value (2.9×10^{-3} cm^2 V^{-1} s^{-1}). After that, the laser annealing at 102 mJ cm^{-2} (per pulse) decreased $\varphi\sum\mu_{max}$. Hence, it was found out that $\varphi\sum\mu_{max}$ of **2** was decreased through laser annealing at too high energy. The color of the sample changed from wine red to black.

Next, to perform closer analysis of such interesting phenomena, the simpler compound **3** possessing a

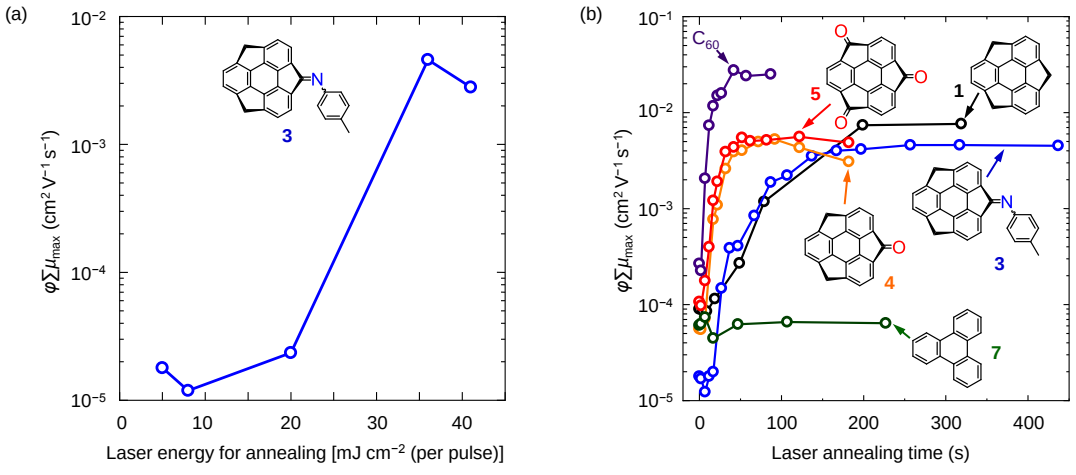

Figure 1−3. (a) Dependence of $\varphi\sum\mu_{max}$ on laser energy for annealing for the laser-annealed film of **3**. (b) Laser annealing time dependence of $\varphi\sum\mu_{max}$ for the laser-annealed film of **1**, **3**, **4**, **5**, **7**, and C_{60}. The laser energy for laser annealing was fixed at 36 mJ cm^{-2} (per pulse).

sumanene skeleton and imino moiety was selected as an appropriate starting material. The following experiments closely examined dependence of $\varphi\sum\mu_{max}$ for **3** on energy and time for laser annealing. Dependence of $\varphi\sum\mu_{max}$ on laser energy for annealing was shown in Figure 1−3a. Although obvious change in $\varphi\sum\mu_{max}$ was not observed below 20 mJ cm^{-2} (per pulse),[4] $\varphi\sum\mu_{max}$ was drastically increased (4.6×10^{-3} cm^2 V^{-1} s^{-1}) at 36 mJ cm^{-2} (per pulse). In contrast, $\varphi\sum\mu_{max}$ was decreased (2.8×10^{-3} cm^2 V^{-1} s^{-1}) at 41 mJ cm^{-2} (per pulse). These results suggested that the threshold energy for laser annealing that can provide increase of the conductivity lies within 20−36 mJ cm^{-2} (per pulse).

Figure 1−3b shows dependence of $\varphi\sum\mu_{max}$ on laser annealing time when laser energy for annealing was fixed at 36 mJ cm^{-2} (per pulse). The value of $\varphi\sum\mu_{max}$ for **3** before laser annealing was similar with that for **2** (1.8×10^{-5} cm^2 V^{-1} s^{-1}). Although the laser annealing for 7 s decreased $\varphi\sum\mu_{max}$, the additional laser annealing for 5 s reverted it back to the original value. After that, $\varphi\sum\mu_{max}$ was suddenly increased to saturate (4.6×10^{-3} cm^2 V^{-1} s^{-1}) through laser annealing for ~3 min in total. The color of the substrate **2** became from yellow to black. This result indicates that the laser annealing made the structure of **3** change to the compound having more conductivity in a molecular level, implying laser annealing prompted growth of sp^2-carbon-rich clusters. Detection of such clusters was dealt in the next chapter, 2−1−1.

Finally, to reveal the properties of laser-induced carbonization for other strained or planar molecules, the similar experiments were also conducted for sumanene (**1**), sumanenemonoone imine **3**, monooxosumanene **4**, trioxosumanene **5**, triphenylene (**7**), and fullerene C_{60} (Figure 1−3b). The behavior of $\varphi\sum\mu_{max}$ for **1** to laser annealing time was almost similar with that for **3**. The dependence curve for **4** was similar to that of **5**. $\varphi\sum\mu_{max}$ for **4** and **5** (5.3×10^{-3} and 5.6×10^{-3} cm^2 V^{-1} s^{-1}, respectively) saturated faster than that for **1** to reach on the order of that for **1** (7.6×10^{-3} cm^2 V^{-1} s^{-1}), suggesting that oxosumanenes **4** and **5** have better efficiency in laser-induced carbonization than **1** under the annealing conditions. Moreover, $\varphi\sum\mu_{max}$ for fullerene C_{60} more rapidly reached to the saturation value (2.8×10^{-2} cm^2 V^{-1} s^{-1}) than that for **1** and **3**–**5**, while that of triphenylene (**7**) did not show a notable change.

1−2−2. Dependence of Electrical Conductivity on Laser Annealing Time in Laser-induced Carbonization of Sumanene Derivatives[1]

In the previous section, the reactions involving laser-induced carbonization were followed through conductivity change in nanometer scale for sumanene derivatives. In contrast, in this section, to research the usability of sumanenemonoone imine **3** as a conducting material, the electrical conductivity was measured during laser annealing in a submillimeter scale using the DC method. The following experiments were done under ambient pressure, temperature, and atmosphere in order to evaluate the conductivity under the environmental conditions. The CH_2Cl_2 solution of **3** was dropped onto a glass substrate with a pair of indium tin oxide (ITO) electrodes with a 200 μm gap and dried under vacuum to form a drop-casted film (Figure 1−4a). The sample was covered with a quartz substrate and fixed with clips to prevent for the film to be scattered due to laser ablation. The sample was exposed to the Nd:YAG laser [wavelength: 355 nm, pulse duration: 5−8 ns, pulse repetition rate: 10 Hz] identical to that of the previous subsection (1−2−1), where laser energy for annealing was stepwise increased. To monitor the conductivity of the sample, electrical resistivity measurements were inserted during laser annealing after removing the cover (Figures 1−4b and c). First, laser annealing was performed at the energy of 36 mJ cm^{-2} (per pulse) because it was confirmed in the previous subsection (1−2−1)

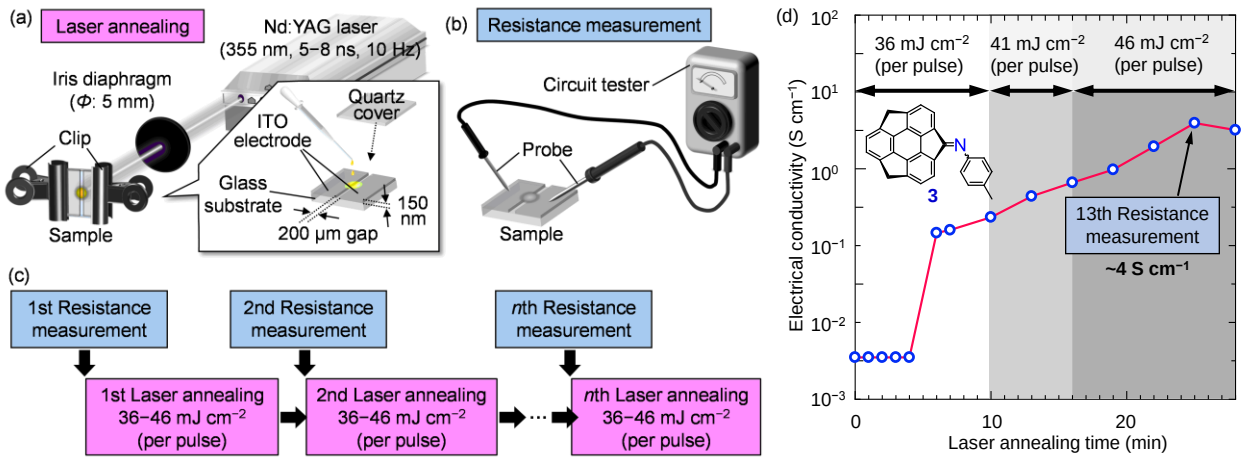

Figure 1−4. Schematic illustration for (a) laser annealing, where (b) resistance measurements were inserted to monitor the conductivity change. The balloon exhibits preparation of sample films drop-casted from a CH_2Cl_2 solution of **3**. (c) Experimental sequence to investigate laser annealing time dependence of conductivity for **3**. (d) Laser annealing time dependence of electrical conductivity for the laser-annealed film of **3**. White, gray, and dark gray tracks represent the laser energy for laser annealing: 36, 41, and 46 mJcm^{-2} (per pulse), respectively.

that the laser annealing at this energy can increase the conductivity of **3**. Although the needle on a circuit tester did not move for the first 4 min, the resistance was abruptly decreased through additional annealing. After that, the laser annealing [41 and 46 mJ cm^{-2} (per pulse)] for 25 min in total made the resistance local minimum. These resistance values were converted into electrical conductivities and plotted against laser annealing time (Figure 1−4d). The local maximum of the conductivity was ~4 S cm^{-1}, which was on the order of that for typical conducting polymers after doping treatment.

1−3. Conclusion

In this chapter, the reactions involving laser-induced carbonization were followed for sumanene derivatives in nanometer and submillimeter scale. As a result, it turned out that the TRMC of C_{60} and sumanene derivatives **1**, **3**−**5** was increased and saturated in this order through laser annealing in contrast to triphenylene (**7**) without obvious change under the laser annealing conditions. In addition, it was suggested that laser-annealed sumanene derivative **3** has potential for conducting materials.

1−4. Experimental Section

General Method

^{1}H (400 MHz) and ^{13}C (100 MHz) NMR spectra were measured on a JEOL JNM-ECS 400 spectrometer. $CDCl_3$ was used as a solvent. The residual $CHCl_3$ peak (δ = 7.26 and 77.0) was used as references for ^{1}H or ^{13}C NMR, respectively. Infrared spectra were recorded on an IR spectrometer (JASCO FT/IR-480plus). Mass spectra were measured on a mass spectrometer (JEOL JMS-DX-303) employing fast atom bombardment (FAB) mode, respectively. Reagents were purchased from commercial sources and used without further purification unless otherwise indicated.

Materials

In this chapter, the compounds **1**−**7**, and C_{60} were dealt for the experiments. Sumanene (**1**),[5]

monooxosumanene **4**,[6] and trioxosumanene **5**[6] were synthesized according to the previously reported procedures. Sumanene imine derivatives **2** and **3** were synthesized through the following procedures. C_{60} and triphenylene (**7**) were purchased from commercial sources and used without further purification.

Synthesis

Sumanenemonoone imine 2

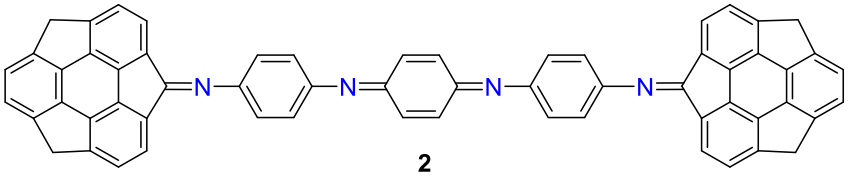

2

To a dried two-necked flask were added $\mathbf{2}_{red}$ (14 mg, 0.0173 mmol), Ag_2O (16.0 mg, 0.0691 mmol), and THF (5 mL) at room temperature under argon. The mixture was stirred for 22 h at room temperature. The mixture was poured into CH_2Cl_2 and a mixed solution (saturated $Na_2S_2O_3$ aq/saturated $NaHCO_3$ aq = 2/1). The aqueous layer was extracted with CH_2Cl_2. The organic layer was filtered off through Na_2SO_4, followed by washing with H_2O and brine, and drying over Na_2SO_4. After evaporation, the crude product (17 mg) was purified by reprecipitation with CH_2Cl_2/hexane. **2** was obtained in 84% yield (11.7 mg, 0.0145 mmol) as a wine red solid: ^{1}H NMR (400 MHz, $CDCl_3$) δ = 7.51 (d, J = 7.8 Hz, 1H), 7.49 (d, J = 7.3 Hz, 1H), 7.31-7.21 (m, 6H), 7.20-7.00 (m, 12H), 6.89 (d, J = 7.8 Hz, 1H), 6.87 (d, J = 7.8 Hz, 1H), 6.41 (d, J = 7.8 Hz, 1H), 6.38 (d, J = 7.8 Hz, 1H), 4.75 (d, J = 20.2 Hz, 1H), 4.745 (d, J = 20.2 Hz, 1H), 4.664 (d, J = 20.2 Hz, 1H), 4.658 (d, J = 19.7 Hz, 1H), 3.514 (d, J = 20.2 Hz, 1H), 3.505 (d, J = 20.2 Hz, 1H), 3.44 (d, J = 19.7 Hz, 1H), 3.43 (d, J = 20.2 Hz, 1H); ^{13}C NMR (100 MHz, $CDCl_3$) δ = 164.77, 158.56, 158.55, 154.20, 153.57, 148.99, 148.97, 148.77, 148.71, 148.69, 148.62, 148.37, 148.32, 147.48, 147.41, 142.14, 142.10, 138.07, 136.71, 136.11, 136.08, 125.40, 125.37, 125.35, 124.87, 124.70, 124.54, 124.09, 123.89, 123.55, 122.42, 122.40, 121.65, 121.62, 42.10, 42.02 ppm; IR (KBr) 3050, 2921, 1721, 1643, 1620, 1590, 1486, 1318, 1260, 1227, 1103 cm^{-1}; HRMS (FAB) Found: *m/z* 808.2611; calcd for $C_{60}H_{32}N_4$: 808.2627.

Sumanenemonoone imine 2_{red}

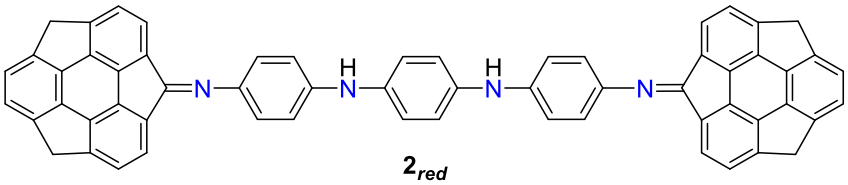

2_{red}

A dried reaction apparatus was equipped with a solvent reservoir set with an activated MS4A (pellet, 1.0 g), reflux condenser, and dried 20 mL two-necked flask (see diagram below). Monooxosumanene **4** (25.4 mg, 0.108 mmol), N^1,$N^{1'}$-(1,4-phenylene)bis(benzene-1,4-diamine) (15.6 mg, 0.0537 mmol), and toluene (5 mL) were added to the flask. The mixture was stirred at 145−153 ˚C for 22 h under argon. During the reaction, the following operation was repeated several times: once the solvent was entirely evaporated out through path 1, the solvent in the reservoir was returned to the flask from path 2 through the MS4A by opening the cock 1. In the first 1 h, this operation was repeated once at ~3 min. In the next 6 h, this operation was repeated once at ~30 min. Then, the cock 1 was kept closed for 10.5 h. After that, this dehydration operation was again repeated once at ~30 min in the final 4.5 h. The reaction mixture was evaporated *in vacuo* and the residue was purified by silica gel column chromatography (CH_2Cl_2/ethyl acetate = 100/0 ~ 80/20) to give **2_{red}** (29.3 mg, 0.0361 mmol, 80%) as a wine red solid: ^{1}H NMR (400 MHz, $CDCl_3$) δ = 7.50 (d, *J* = 7.8 Hz, 2H), 7.23 (d, *J* = 7.4 Hz, 2H), 7.21-7.24 (bs, 4H), 7.15 (d, *J* = 7.8 Hz, 2H), 7.12 (d, *J* = 7.8 Hz, 2H), 7.13-7.16 (bs, 4H), 7.08 (bs, 4H), 6.91 (d, *J* = 7.3 Hz, 2H), 6.58 (d, *J* = 7.8 Hz, 2H), 5.72 (bs, 2H), 4.74 (d, *J* = 20.2 Hz, 2H), 4.67 (d, *J* = 20.2 Hz, 2H), 3.50 (d, *J* = 20.2 Hz, 2H), 3.44 (d, *J* = 20.2 Hz, 2H); ^{13}C NMR (150 MHz, $CDCl_3$) δ = 163.15, 153.74, 152.95, 148.90, 148.74, 148.64, 148.52, 148.64, 148.35, 148.18, 148.05, 142.54, 136.04, 124.64, 124.60, 123.84, 123.61, 123.01, 122.75, 122.65, 120.73, 120.61, 116.96, 116.90, 41.91, 41.86 ppm; IR (KBr) 3396, 3046, 2928, 1720, 1616, 1499, 1395, 1303, 1253, 1227, 1168 cm^{-1}; HRMS (FAB) Found: *m/z* 810.2794; calcd for $C_{60}H_{34}N_4$: 810.2783.

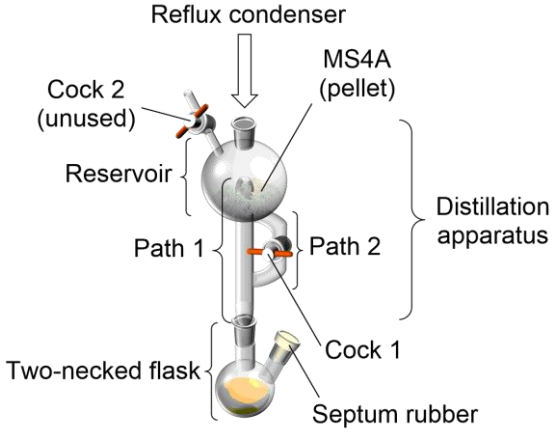

Sumanenemonoone imine 3

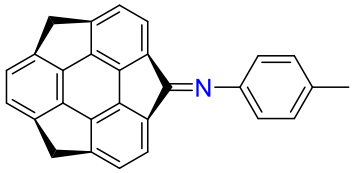

3

A dried round-bottomed flask equipped with a magnetic stirring bar and activated molecular sieves (MS4A, 0.5 g) was charged with monooxosumanene **4** (6.2 mg, 0.022 mmol) and *p*-toluidine (10.0 mg, 0.093 mmol). After evacuation purging with argon, absolute CH_2Cl_2 (5 mL) was added to the mixture. The reaction mixture was heated to 40 °C and stirred for 3 h under argon. After that, the activated molecular sieves (MS4A, 0.5 g) were added again under argon flow and the mixture was stirred for 2 h under argon. The reaction mixture was cooled to room temperature, and then filtered through a cotton plug. The filtrate was evaporated *in vacuo*. The residue was purified by silica-gel column chromatography (dichloromethane/hexane = 70/30 ~ 100/0) to give sumanenemonoone imine **3** as a yellow solid (8.2 mg, 0.022 mmol, 100%). ^{1}H NMR (400 MHz, $CDCl_3$): δ = 7.48 (d, J = 7.3 Hz, 1H), 7.21-7.25 (m, 3H), 7.09-7.15 (m, 4H), 6.84 (d, J = 7.3 Hz, 1H), 6.27 (d, J = 7.3 Hz, 1H), 4.73 (d, J = 19.7 Hz, 1H), 4.64 (d, J = 20.2 Hz, 1H), 3.49 (d, J = 20.2 Hz, 1H), 3.31 (d, J = 19.7 Hz, 1H), 2.42 (s, 3H) ppm; ^{13}C NMR (100 MHz, $CDCl_3$): δ = 164.18, 153.73, 153.17, 148.83, 148.74, 148.62, 148.49 ×2, 148.39, 148.32, 148.19, 148.15, 142.14, 136.11, 134.75, 129.74, 125.20, 124.65, 124.43, 123.84, 123.64, 123.26, 120.43, 41.91, 41.84, 21.10 ppm; IR (ATR, powder): 1624 (C=N) cm^{-1}; UV-Vis-NIR (transmission measurement, thin film): λ_{max}: 273, 410 nm; HRMS (FAB): calcd for $C_{28}H_{17}N$: 367.1361, Found: *m/z* 367.1350 [M^+].

Conductivity Measurements

TRMC measurements

TRMC was measured according to a previously reported procedure.[3] In the text, the preparation of the sample film and experimental parameters for the laser are described in detail. The input power of the microwave was ~3 mW, and the frequency was ~9 GHz. Each TRMC measurement was carried out just after the laser annealing.

Electrical conductivity measurements

Because the laser annealing process is detailed in the text, the measured values of the electrical resistance and calculated conductivity are summarized in Table 1−1 as a function of total time of laser annealing. The resistance was measured using a circuit tester (CUSTOM, CX-180N) by a two-probe method.

Table 1−1. Dependence of electrical resistance and conductivity on laser annealing time

Pulse energy [mJ cm^{-2} (per pulse)]	36								41		46			
Annealing time (min)[a]	0	1	2	3	4	6	7	10	13	16	19	22	25	28
Resistance (Ω)	$>10^6$	$>10^6$	$>10^6$	$>10^6$	$>10^6$	2.4×10^4	2.2×10^4	1.5×10^4	8.0×10^3	5.3×10^3	3.6×10^3	1.8×10^3	8.9×10^2	1.1×10^3
Conductivity (S cm^{-1})	<4	<4	<4	<4	<4	0.2	0.2	0.2	0.4	0.7	1	2	4	3

[a] Total time

1−5. References and Notes

[1] a) J. I. Raffel, J. F. Freidin, G. H. Chapman, *Appl. Phys. Lett.* **1983**, *42*, 705-706; b) C. Decker, *J. Polym. Sci., Part C: Polym. Lett.* **1987**, *25*, 5-10; c) M. Schumann, R. Sauerbrey, M. C. Smayling, *Appl. Phys. Lett.* **1991**, *58*, 428-430; d) S. Kawanishi, Y. Shimizu, S. Sugimoto, N. Suzuki, *Polymer* **1991**, *32*, 979-983; e) H. M. Phillips, D. Sarkar, N. J. Halas, R. H. Hauge, R. Sauerbrey, *Appl. Phys. A: Solids Surf.* **1993**, *57*, 105-107; f) R. Srinivasan, R. R. Hall, D. C. Allbee, *Appl. Phys. Lett.* **1993**, *63*, 3382-3383; g) M. Ferretti, A. Parisini, M. Manfredini, P. Milani, *Chem. Phys. Lett.* **1996**, *259*, 432-437; h) D. Ning, Q. H. Lou, J. X. Dong, Y. R. Wei, *Appl. Phys. A* **1996**, *62*, 509-512; i) R. Kostecki, X. Song, K. Kinoshita, *Electrochem. Solid-State Lett.* **2002**, *5*, E29-E31; j) J. I. Inoue, H. Wada, T. Mori, *Jpn. J. Appl. Phys.* **2010**, *49*, 0716051-0716055.

[2] Z. Y. Qin, B. Y. Du, J. Zhang, T. B. He, L. Qin, Y. S. Zhang, *Appl. Phys. A* **2001**, *72*, 711-715.

[3] S. Seki, A. Saeki, T. Sakurai, D. Sakamaki, *PCCP* **2014**, *16*, 11093-11113.

[4] Y. Shimizu, *Master thesis* **2010**.

[5] H. Sakurai, T. Daiko, T. Hirao, *Science* **2003**, *301*, 1878.

[6] T. Amaya, M. Hifumi, M. Okada, Y. Shimizu, T. Moriuchi, K. Segawa, Y. Ando, T. Hirao, *J. Org. Chem.* **2011**, *76*, 8049-8052.

Chapter 2. Structural and Catalytic Properties of the Carbonized Product through Laser Annealing of Sumanene Derivatives[1,5]

2−1. Introduction

Nitrogen-doped graphitic carbons (NGCs), where nitrogen atoms are doped into graphitic lattice, have been researched due to their interesting electrical and catalytic properties. Recently, they have been especially studied as cathode catalysts of polymer electrolyte fuel cells.[1] The ratio of nitrogen atoms to carbon ones (N/C ratio) and the binding state of nitrogen atoms in graphitic lattice are one of the large effective factors toward material properties of NGCs.[2] As described in General Introduction, the widely-used synthetic method of NGCs is pyrolysis of nitrogen-containing compounds including organic small-molecule compounds,[3] ionic liquids,[4] and polymers.[5] NGCs are typically obtained through pyrolysis of such nitrogen-containing compounds at the temperature in the range of 600−1000 °C.[6] In this method, it was reported that nitrogen atoms generally started eliminating above ~600 °C,[7] implying that retention of N/C ratio is difficult.

NGCs can work as catalysts of oxygen reduction reaction (ORR) in fuel cells. When an NGC is employed as a cathode, oxygen gas is reduced with electrons in the presence of protons on the surface. The values to be often used in the discussion of evaluation of ORR activity are ORR onset potential (E_{onset}) and limiting current density (i_L) as shown in Table 2−1. The larger these values become, the larger voltage and current can be obtained from the cell.[1]

The conductivity increase of sumanene derivatives through laser annealing was dealt in Chapter 1. This chapter focuses on the confirmation of such phenomenon based on the laser-induced carbonization through structural analysis of the laser-annealed product. Here, sumanenemonoone imine **3** was employed as a starting material. The structure of the carbonous product was analyzed by Raman spectroscopy, grazing-incidence X-ray diffractometry (GI-XRD), and X-ray photoelectron spectroscopy (XPS). Moreover, ORR activity was also measured in view of applicability to catalytic materials. In Table 2−1, some evaluation objects and viewpoints were briefly summarized in each analysis method.

Table 2−1. Measurement methods employed and the evaluation objects and viewpoints for structural and catalytic characterization of laser-annealed **3**.

	Structural property			Catalytic property
	Raman	XRD	XPS	ORR
Evaluation object	Existence and size of graphitic lattice	Size and orientation of graphitic lattice	N/C ratio and bonding state of nitrogen atoms	Catalytic activity to ORR
	・G band (~1600 cm^{-1}): Graphitic lattice ・D band (~1350 cm^{-1}): sp^3-bonded carbon, structural defects	・(002) peak (~26 °) ・(10) peak (~42 °)	・C 1s core level peak (~285 eV) ・N 1s core level peak (~400 eV)	Onset potential: E_{onset} Limiting current density: i_L
Viewpoints	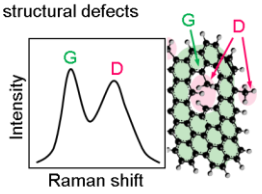	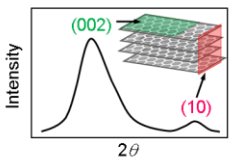	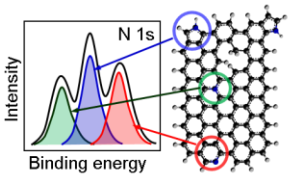	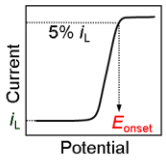

2−2. Results and Discussion

2−2−1. Raman Spectroscopic Analysis of Laser-annealed Sumanenemonoone imine 3[1]

Raman spectroscopy is one of the useful methods to characterize carbonous materials. In this method, inclusion of graphitic lattice within a sample can be confirmed through detecting G band (~1600 cm^{-1}) characteristic to vibrational mode of lattice consisting of fused aromatic rings (Table 2−1).[8] Therefore, detection of G band leads to confirming that the conductivity increase of sumanene derivatives through laser annealing is caused by laser-induced carbonization. In this subsection, Raman spectroscopic analysis was carried out for laser-annealed sumanenemonoone imine **3**. A spin-coated film of **3** on an ITO/glass substrate was covered with a slide glass and annealed with a Nd:YAG laser [355 nm, 5−8 ns, 12 Hz, 44 mJ cm^{-2} (per pulse)] (Figure 2−1a). The color of the film changed from yellow to black and the film thickness decreased from ~100 nm to ~80 nm. 532 nm laser excitation of the laser-annealed sample generated Raman scattered light, which was detected through an objective lens. Thus-obtained Raman spectrum included the D band (~1335 cm^{-1}) attributed to structural defects or sp^3-bonded carbons[9] in addition to the above-mentioned G band (~1590 cm^{-1}) as shown in Figure 2−1b. The spectrum is similar to the carbonous compounds synthesized through pyrolysis at 700−1500 °C.[10] It is reported that the carbonous compounds obtained through laser annealing are available as electrodes even though they include such structural defects,[11] although heat treatment above

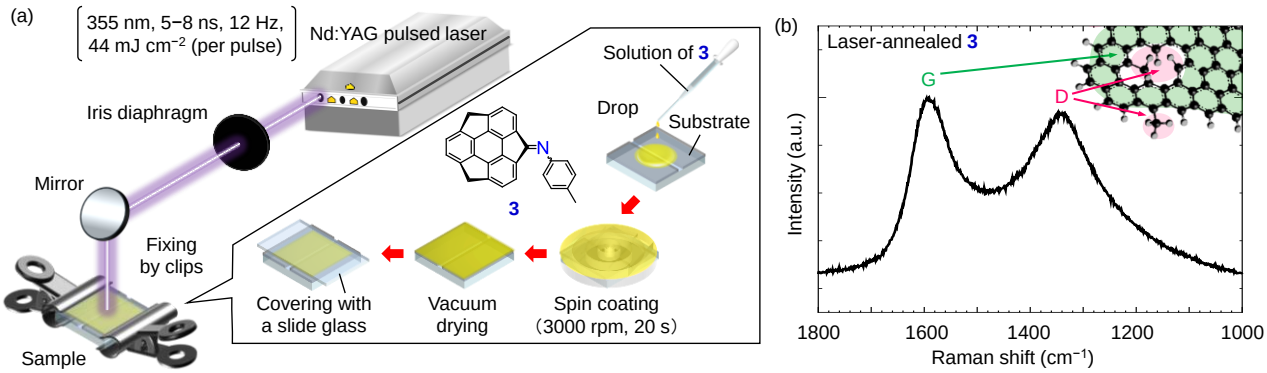

Figure 2−1. (a) Schematic illustration for preparation of laser-annealed **3** film formed by spin-coating method on an ITO/glass substrate. (b) Raman spectrum of the laser-annealed **3** film. Top-right inset expresses schematic illustration of graphitic carbon lattice with sp^3-bonded carbons and structural defects. G and D above the spectrum represent G and D bands, respectively.

2000 °C is necessary so as to suppress the structural defects. To estimate the size of graphitic lattice, the ratio of intensity or area between G and D band is often used.[12] In this case, however, such a method is considered to be inappropriate because the two bands are not separated well. It is experimentally known that there is a relationship between full width at half maximum (FWHM) and the size of graphitic lattice in such carbonous compounds.[12] According to the relationship, the size of graphitic lattice in the laser-annealed film of **3** was estimated to be on the order of 1−10 nm because the observed FWHM of the film was ~100 cm^{-1}. Therefore, the presented film includes graphitic lattice with structural defects, which is a strong evidence for the laser-induced carbonization of **3**.

2−2−2. Grazing Incidence X-ray Diffraction (GI-XRD) Analysis of Laser-annealed Sumanenemonoone imine 3[1]

In this subsection, GI-XRD analysis was conducted to obtain the information about the size of graphitic lattice and its orientation for the above-mentioned film synthesized through laser-induced carbonization of **3**. The diffracted X-ray was detected by sweeping a detector, where the incident angle of the X-ray was fixed at an extremely small value of 0.08 ° (2θ–scan). This is because the film thickness of the presented sample is smaller than the penetration depth of the X-ray employed. The measurement was carried out in an out-of-plane configuration, which provides information about diffraction from lattice plane parallel to the substrate. The

resulting spectrum bore broad peaks at ~24 ° and ~42 °, which are considered to be assigned to (002) and (10) plane of graphitic crystallites (Figure 2−2a). The crystallites are not likely to be oriented because these two peaks were observed at the same time even though the incident angle of the X-ray was fixed. The average size of the graphitic crystallites was estimated at ~5 nm using Scherrer's equation,[13] where the shape factor employed was 1. This result is in good agreement with that obtained from Raman spectroscopic analysis in the previous subsection. Moreover, the peak position of (002) plane observed in the sample (~24 °) was shifted to lower angle as compared to that observed in graphite (~26 °). This shift is interpreted as due to expansion of interplanar spacing of the graphitic crystallites, suggesting the formation of turbostratic structures, which represent basal planes that have slipped out of the crystal structure alignment.[14] This result also corresponds to the detection of D band in the Raman measurement in the previous subsection.

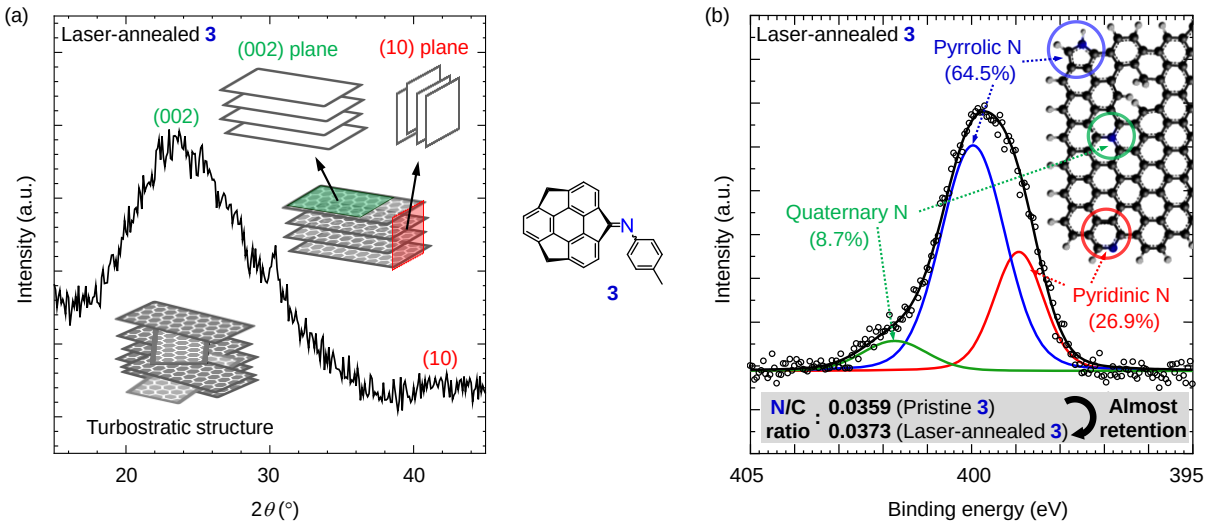

Figure 2−2. (a) GI-XRD and (b) XPS spectra of the laser-annealed **3** film. Top-right and bottom-left insets in (a) display schematic illustration of graphitic carbon lattice with (002) and (10) plane, and turbostratic structure, respectively. Top-right inset in (b) depicts schematic diagram of nitrogen-doped graphitic carbon including pyridinic, pyrrolic, and quaternary (graphitic) nitrogen atoms. The N 1s spectrum was deconvoluted into the three components corresponding to the nitrogen atoms. White circles represent measurement data, where the background was subtracted using linear function and Shirley method. N/C ratios of pristine and laser-annealed **3** are listed below the N 1s spectra.

2−2−3. X-ray Photoelectron Spectroscopy (XPS) Analysis of Laser-annealed Sumanenemonoone Imine 3[1]

The carbonous compound produced through laser-induced carbonization is likely to include nitrogen atoms because the starting material, sumanenemonoone imine **3** possesses a nitrogen atom. In this subsection, nitrogen atoms in the product were focused on. The XPS analysis explored the information about the content and binding states of nitrogen atoms. In this method, binding energy of electrons is provided by observing kinetic energy of photoelectrons emitted from electron shells through X-ray irradiation under ultra-high vacuum. The peak position reflects difference of atoms and their binding states because binding energy of photoelectrons depends on these factors. The sample employed in the measurements was the laser-annealed film of sumanenemonoone imine **3** described in subsection 2−2−1. The binding energy of the film was surveyed for C 1s and N 1s core level. As a result, C 1s (~284.6 eV) and N 1s (~399.8 eV) peaks were observed, showing existence of nitrogen atoms in the sample. Figure 2−2b shows the N 1s core level XPS spectrum. Deconvolution of the N 1s peak generated three peaks corresponding to pyridinic, pyrrolic, and quaternary (graphitic) nitrogen atoms, implying that such types of nitrogen atoms are included in the sample. The ratio of each component was calculated at 26.9: 64.5: 8.7, respectively. Because pyrrolic nitrogen atom was a major component, the achieved temperature was presumed to be below ~600 °C under the present laser parameters.[15] The N/C ratio of the laser-annealed product of **3** was estimated at 0.0373, while that of the starting material **3** itself was done at 0.0359, showing almost the retention, although the value increased by only 3.9%. This result contrasts with that of NGC synthesis through general pyrolysis above ~600 °C, which largely decreases N/C ratio of the resulting NGC as described in the introduction of this chapter. Hence, the suppression of elimination of nitrogen atoms implies that sumanenemonoone imine **3** is susceptible to laser-induced carbonization, which was closely studied in Chapter 3.

2−2−4. Oxygen Reduction Reaction (ORR) Activity of Laser-annealed Sumanene Imine Derivatives[5]

The previous subsection revealed that NGC was formed through laser-induced carbonization of

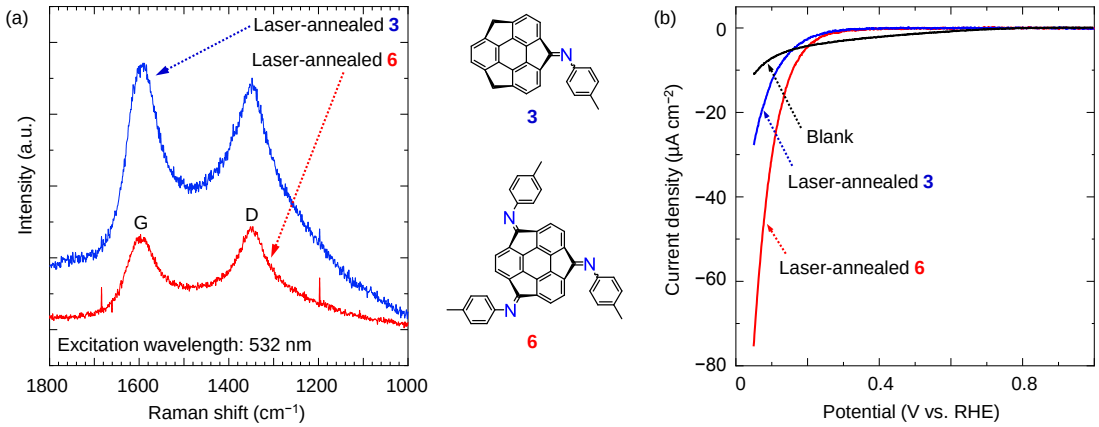

Figure 2−3. (a) Raman spectra and (b) ORR polarization curve at 300 rpm of laser-annealed **3** and **6**. Blank data are also drawn in (b) for comparison.

sumanenemonoone imine **3**. This subsection studied the ORR activity of the carbonous products through laser-induced carbonization of sumanenemonoone imine **3** (theoretical N/C ratio: 0.0357) and sumanenetrione triimine **6** (theoretical N/C ratio: 0.0714). In this experiment, NGCs were directly synthesized on the surface of the glassy carbon electrode (disk) of a rotating ring disk electrode through laser-induced annealing of the drop-casted film of **3** or **6**. The laser parameters were set as follows, wavelength: 355 nm, pulse duration: 5−8 ns, pulse repetition rate: 12 Hz, energy: 42−45 mJ cm^{-2} (per pulse). For both samples, the electrical resistance measurements confirmed electrical contact between the laser-annealed product and disk electrode because the film resistance was decreased and saturated during the laser annealing (see experimental section). Moreover, Raman spectroscopic analysis supported the carbonization of **3** and **6** through detection of G and D bands (Figure 2−3a). N/C ratio and binding states of nitrogen atoms were not examined because the electrode bearing the sample were too large to be inserted into the measuring chamber of an XPS spectrometer.

Cyclic voltammetry measurements were conducted in oxygen saturated 0.1 M H_2SO_4 aq. to examine the behavior of the carbonous products as cathodes. Figure 2−3b exhibits the ORR polarization curves. The carbonous products synthesized through laser-induced carbonization of **3** and **6** showed slight activity toward ORR, which is higher than that of the blank conditions. The values of E_{onset} and i_L of these samples could not be evaluated because they were much smaller than those of platinum-supported carbon electrodes and NGCs.[1] E_{onset} of the carbonous product derived from **6** was higher than that derived from **3**. As one of the possibilities,

this is maybe because the former product is considered to include more nitrogen atoms than the latter one. The ORR activity was not measured below 0 V because the electrolyte itself reacted on the disk electrode without a catalyst.

2−3. Conclusion

In summary, this chapter explored the structural and catalytic properties of the products generated by laser annealing of nitrogen-containing sumanene derivatives. These results suggest that sumanenemonoone imine **3** was transformed to carbonous compound with nitrogen atoms, structural defects, and turbostratic structure through laser annealing. The conductivity increase discussed in Chapter 1 is considered to be caused by growth of sp^2-carbon-rich cluster in nanometer scale, confirming that the phenomena are based on laser-induced carbonization. Moreover, the ORR measurements of the carbonous products derived from laser-induced carbonization of sumanene derivatives **3** and **6** showed slight ORR activity.

2−4. Experimental Section

General Method

^{1}H (400 MHz) and ^{13}C (100 MHz) NMR spectra were measured on a JEOL JNM-ECS 400 spectrometer. CD_2Cl_2 was used as a solvent. The residual CH_2Cl_2 and $CDHCl_2$ peaks (δ = 5.32 and 53.8) were used as references for ^{1}H or ^{13}C NMR, respectively. Infrared spectra were recorded on an IR spectrometer (JASCO FT/IR-480plus). Mass spectra were measured on a mass spectrometer (BRUKER AUTOFLEX III). Reagents were purchased from commercial sources and used without further purification unless otherwise indicated.

Materials

This chapter dealt the compounds **3** and **6** for the experiments. Synthesis of **3** was described in Chapter 1. Sumanenetrione triimine **6** was synthesized through the following procedures.

Synthesis

Sumanenetrione triimine 6

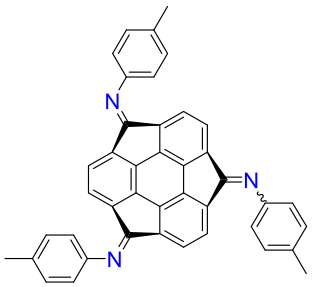

6

Trioxosumanene **5**[16] (10.3 mg, 33.6 µmol) and *p*-toluidine (21.6 mg, 20.2 µmol, 6 eq.) were charged to a dried round-bottomed flask equipped with a magnetic stirring bar and activated molecular sieves (MS4A, pellet, 0.5 g). After evacuation followed by purging with argon, 10 mL of absolute toluene was added to the mixture. The reaction mixture was heated to 120 °C and stirred for 4 h under argon. After the activated molecular sieves (MS4A, pellet, 0.5 g) were added again to the reaction mixture under argon, the mixture was stirred for 14 h under argon at 120 °C. The reaction mixture was cooled to ambient temperature, and then filtered through a cotton. The filtrate was evaporated *in vacuo*. The residue was purified by preparative thin-layer chromatography (dichloromethane) to give the desired compound **6** as a red-orange solid. Furthermore, the solid was refined by reprecipitation (dichloromethane/cooled hexane) to provide **6** (6.5 mg, 11.3 µmol, 34%) as needle-like red-orange crystals: FT−IR (KBr): ν = 3023, 2921, 2856, 1891, 1719, 1648, 1618, 1560, 1502, 1392, 1327, 1194, 1108, 1016 cm^{-1}; ^{1}H NMR (400 MHz, CD_2Cl_2) δ = 7.62 (d, *J* = 7.7 Hz, 1H), 7.60 (d, *J* = 7.7 Hz, 1H), 7.32−7.21 (m, 6H), 7.21−7.14 (m, 6H), 7.11 (d, *J* = 8.2 Hz, 2H), 7.04 (d, *J* = 8.2 Hz, 2H), 6.99 (d, *J* = 8.2 Hz, 2H), 6.51 (d, *J* = 7.9 Hz, 1H), 6.98 (d, *J* = 7.9 Hz, 1H), 6.10 (d, *J* = 7.9 Hz, 1H), 6.07 (d, *J* = 7.9 Hz, 1H), 2.45 (s, 3H), 2.43 (s, 3H), 2.37 (s, 3H), 2.36 (s, 3H) ppm; ^{13}C NMR (100 MHz, CD_2Cl_2): δ = 163.05, 163.01, 162.92, 162.87, 148.94, 148.76, 148.47, 148.44, 148.37, 148.30, 148.29, 148.27, 148.19, 148.16, 147.93, 147.87, 146.36, 146.04, 145.86, 145.50, 139.77, 139.55, 139.37, 139.11, 136.32, 136.30, 136.17, 136.13, 130.24, 130.22, 130.10, 130.09, 126.78, 126.64, 126.60, 126.52, 124.88, 124.81, 124.66, 124.63, 120.96, 120.90, 120.76, 120.70, 21.21, 21.20, 21.12, 21.11 ppm; HRMS (MALDI−TOF) *m*/*z* calcd for $C_{42}H_{28}N_3^+$ $[M+H]^+$ 574.2278, found 574.2275.

Preparation of laser-annealed sample film

After a CH_2Cl_2 solution of **3** was dropped onto an ITO/glass substrate, the substrate was rotated (3000 rpm, 20 s) and dried under vacuum to form a spin-coated film. The substrate was identical to that employed in the subsection 1−2−2 in the previous chapter. Thus-obtained film was covered with a slide glass and fixed with clips. After that, the film was exposed to a Nd:YAG pulsed laser [355 nm, 5−8 ns, 12 Hz, 44 mJ cm^{-2} (per pulse)]. The film thickness was measured using a surface profiler (Veeco, Dektak150).

Raman spectroscopic analysis of the laser-annealed film of 3

The spectrum was measured by a micro-Raman spectrometer (JASCO, NRS-3100). The 532 nm continuous-wave laser beam was focused on the surface of the sample film through an objective lens (× 100). The exposure time, slit size, and number of scans were 8 s, 0.1 × 6 mm, and twice, respectively.

GI-XRD analysis of the laser-annealed film of 3

The GI-XRD measurement was conducted employing an X-ray diffractometer (Rigaku Corp., SmartLab) under ambient conditions. To accurately measure diffracted X-ray positions excluding the effects derived from sample shape, the parallel beam method was used. The Al Kα line (1486.6 eV) was employed as an X-ray source. The tube current was 200 mA, and the tube voltage was 45 kV. The experimental setup is shown in Figure E2−1a. While the grazing incident angle ω was fixed at 0.08 °, the angle of the detector 2θ was swept from 10

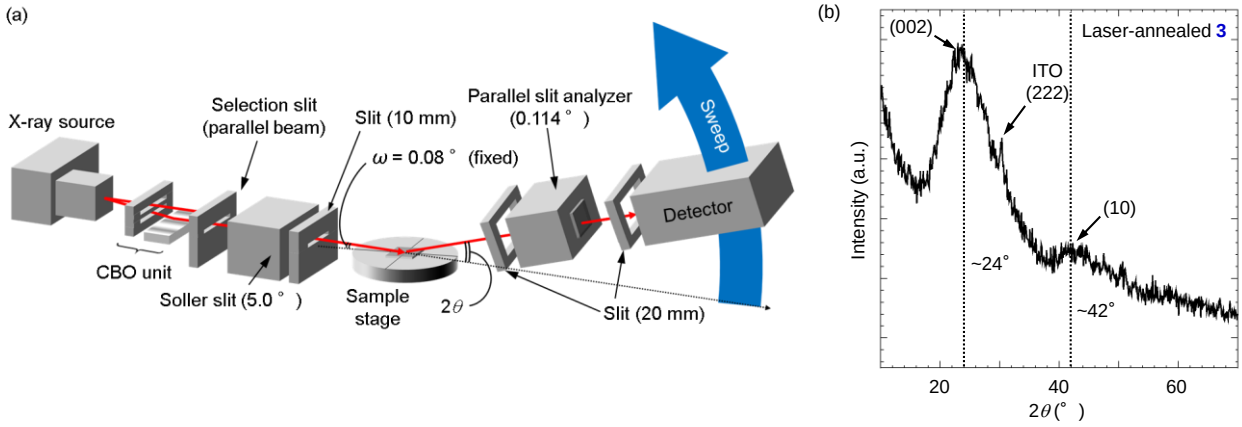

Figure E2−1. (a) Experimental setup of the GI-XRD measurement in the out-of-plane configuration. (b) Wide-range GI-XRD spectrum of the laser-annealed film of **3**.

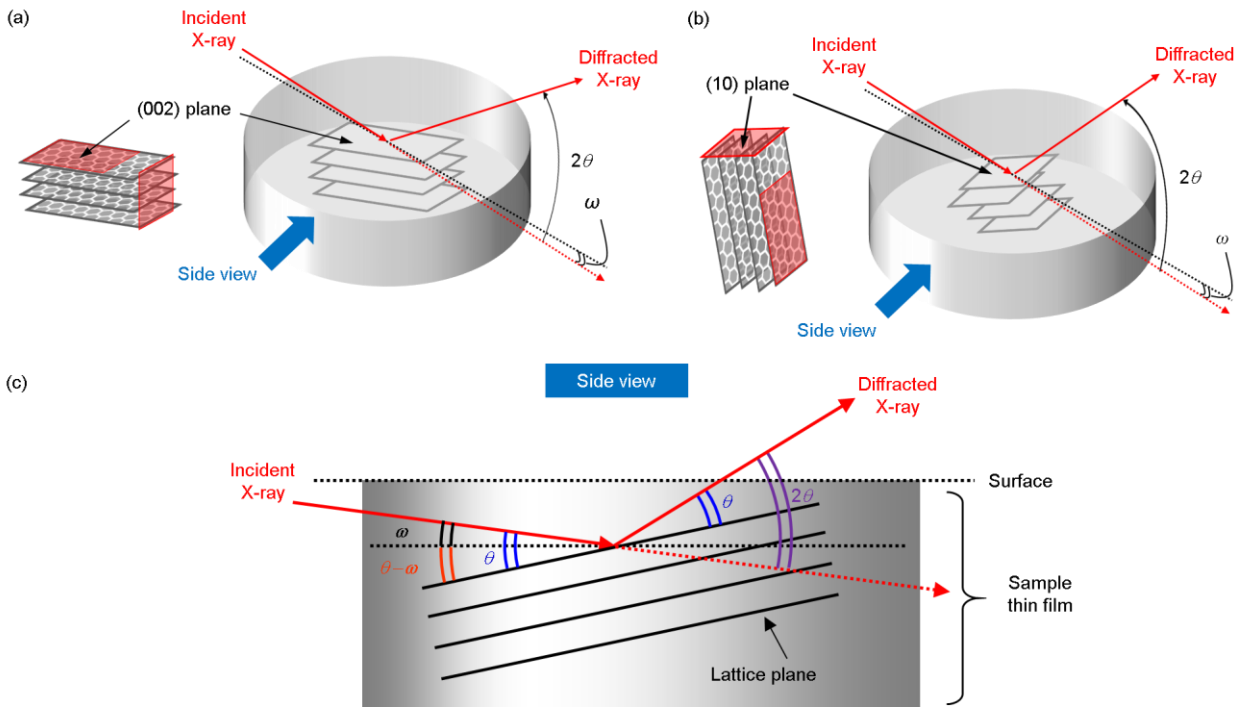

Figure E2−2. Schematic diagrams showing two configurations of a graphitic crystallite when diffraction from the (a) (002) and (b) (10) plane of graphitic crystallites are detected in the measurement. (c) Side view of (a) and (b). The lattice plane is inclined at an angle of $\theta - \omega$ to the sample surface.

to 70 ° at the rate of 10 ° min^{-1} (2θ–scan). The wide-range GI-XRD spectrum obtained is exhibited in Figure E2−1b. In the sample film, graphitic crystallites should be arranged as shown in Figures E2−2a and b in accordance with the measurement results. Because a diffraction peak appears when a value of θ is consistent with Bragg diffraction angle, inclination angle of the lattice plane to the sample surface, $\theta - \omega$ corresponding to the (002) and (10) plane (Figure E2−2c) is calculated to yield ~12 and 21°, respectively.

XPS analysis of the laser-annealed film of 3

The XPS measurement was performed with an X-ray photoemission spectrometer (SHIMADZU Corp./Kratos, AXIS-165x) at room temperature in an ultrahigh-vacuum chamber (~7 × 10^{-8} Pa). The monochromatic Al Kα line (1486.6 eV) was employed as X-ray source. The tube current was 12 mA, and the tube voltage was 15 kV. Before the measurements, the sample surfaces were etched using accelerated argon ion to remove extraneous surface carbon. The emission current was 15 mA, and argon gas pressure was ~2 × 10^{-5} Pa. The binding energies were referenced to Ag $3d_{5/2}$ line (368.2 eV).[17] The intensity (counts s^{-1}) was corrected

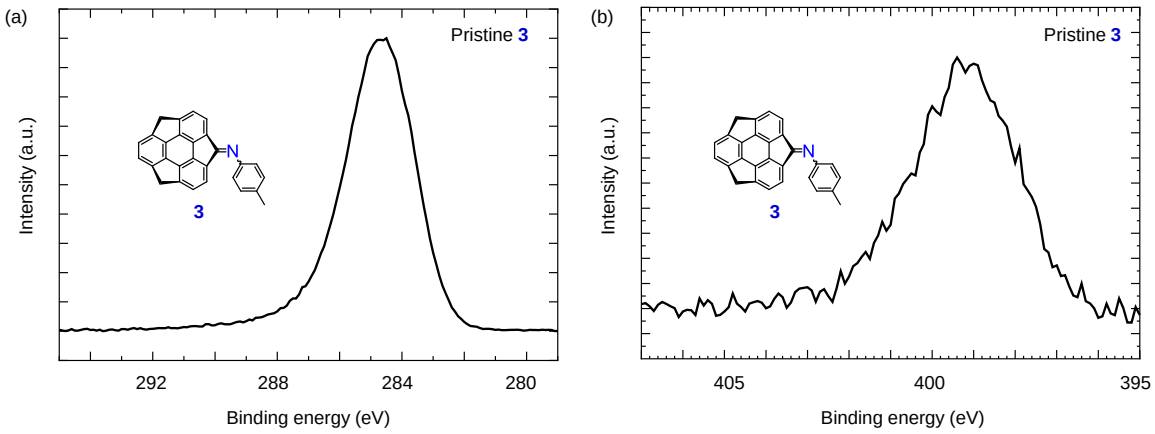

Figure E2−3. (a) C 1s and (b) N 1s XPS spectra of a pristine film of **3** (before laser annealing).

for quantitative analysis employing appropriate transmission values supplied by the instrument manufacturer. Peak analysis of these spectra was carried out using an analysis software (Light Stone, OriginPro). Background of the C1s spectrum was subtracted by Shirley method. On the other hand, background subtraction for N 1s spectrum was conducted in two stages. First, linear function was subtracted from the background to get rid of the gradient of the spectrum, and then the Shirley method was used to the background subtraction. Each XPS spectrum is shown after subtracting the background.

The pass energy was 160 eV. Figure E2−3 shows the C 1s and N 1s spectra of a pristine film of **3** before laser annealing. The N/C ratio estimated from the peak areas (44.114 for C 1s and 1.585 for N 1s) was 0.0359. The pass energy was set at 20 eV to enhance the energy resolution for peak deconvolution. The N 1s spectrum of the laser-annealed film of **3** was shown in Figure 2−2b. The N/C ratio derived from calculation of peak areas (375.124 for C 1s and 14.010 for N 1s) was 0.0373. The N 1s spectrum was fitted with Voigt functions, where Lorentzian width was fixed to 0.25 eV. The deconvolution generated three peaks at 398.9, 400.0, and 401.7 eV attributed to pyridinic, pyrrolic, and quaternary (graphitic) nitrogen atoms, respectively (Figure 2−2b). Each peak area composing the N 1s spectrum was measured to give their ratio (pyridinic / pyrrolic / quaternary = 26.9/ 64.5/8.7).

Direct synthesis of NGCs on a rotating ring disk electrode

A rotating ring disk electrode was employed. The disk electrode was made of glassy carbon and its diameter

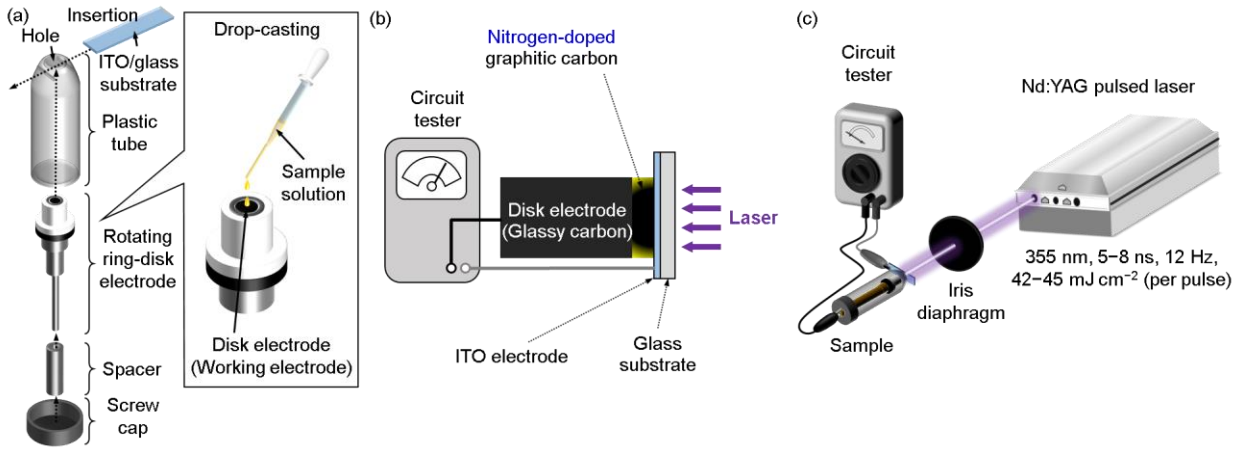

Figure E2−4. (a) Schematic illustration for setup of apparatus to confirm electrical contact between the laser-annealed sample and the disk electrode of a rotating-ring-disk electrode. (b) Cross-sectional diagram of the sample film, which is sandwiched between the ITO and disk electrodes. Nitrogen-doped graphitic carbon formed through laser annealing makes electrical bridge to reduce the film resistance.

was 6 mm. A CH_2Cl_2 solution of **3** or **6** was drop-casted on the disk electrode and dried *in vacuo* (Figure E2−4a).

So as to monitor the progress of carbonization during laser annealing by measuring the electrical resistance, the sample film was sandwiched between the disk electrode and an ITO electrode, and then fixed using a plastic tube and screw cap as shown in Figure E2−4b. The bottom of the tube was hollowed out not to prevent laser annealing. After that, the terminal of the disk electrode and the ITO electrode were connected with a circuit tester using electrical clips (Figure E2−4c). Then, the needle of the tester did not move (> 1MΩ). The measurements of electrical resistance were inserted during laser annealing of the sample employing a Nd:YAG laser [355 nm, 5−8 ns, 12 Hz, 42−45 mJ cm^{-2} (per pulse)]. The dependence of the resistance value on laser annealing time was summarized in Table E2−1 and Figure E2−5. The circuit tester employed here was identical to that used in the DC measurement in Chapter 1.

Table E2−1. Electrical resistance values of the laser-annealed films of (a) **3** and (b) **6** with laser-annealing time.

(a)

Laser exposure time (s)	0	60	90	120	150	180	210	240	270	300	330	360
Resistance (Ω)	>1MΩ	580	290	180	140	100	90	80	78	73	70	69

(b)

Laser exposure time (s)	0	20	30	60	90	120	150	180	210	240	300	360	420
Resistance (Ω)	>1MΩ	6500	4200	2100	390	350	320	280	270	250	240	220	220

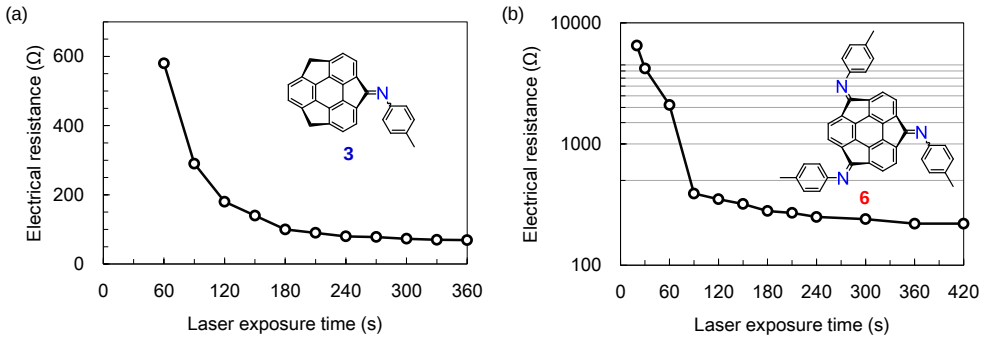

Figure E2−5. Dependence of electrical resistance of the laser-annealed films of (a) **3** and (b) **6** on laser-annealing time.

ORR measurements

The measurements were performed under the following conditions: working electrode: rotating ring disk electrode (glassy carbon disk and platinum ring), disk area: 0.283 cm^2, reference electrode: RHE, counter electrode: platinum wire, electrolyte: 0.1 M H_2SO_4, potential range: 1.0−0.05 V, sweep rate: 50 mV s^{-1} or 5 mV s^{-1}, and rotating rate of the electrode: 300 rpm. Also, the electrodes were polished before the measurements. Hydrogen and nitrogen gas were bubbled for 20 min until saturation in the reference and working electrode, respectively. After the electrodes were electrochemically cleaned by potential sweep (50 mV s^{-1}, 20 cycle), the background was measured (5 mV s^{-1}, 2 cycle). After that, nitrogen gas flow was stopped, and then oxygen gas was bubbled until saturation. Finally, ORR measurements were conducted (5 mV s^{-1}, 2 cycle). The polarization curves in Figure 2−3b were drawn after background subtraction.

2−5. References and Notes

[1] X. Zhou, J. Qiao, L. Yang, J. Zhang, *Adv. Energy Mater.* **2014**, *4*, 1301523.

[2] H. Wang, T. Maiyalagan, X. Wang, *ACS Catal.* **2012**, *2*, 781-794.

[3] D. P. Kim, C. L. Lin, T. Mihalisin, P. Heiney, M. M. Labes, *Chem. Mater.* **1991**, *3*, 686-692.

[4] B. J. P. Paraknowitsch, J. Zhang, D. Su, A. Thomas, M. Antonietti, *Adv. Mater.* **2010**, *22*, 87-92.

[5] a) L. Y. Chiang, J. P. Stokes, D. C. Johnston, D. P. Goshorn, *Synth. Met.* **1989**, *29*, 483-488; b) Z. Morávková, M. Trchová, M. Exnerová, J. Stejskal, *Thin Solid Films* **2012**, *520*, 6088-6094; c) M.

Murakami, H. Yasujima, Y. Yumoto, S. Mizogami, S. Yoshimura, *Solid State Commun.* **1983**, *45*, 1085-1088; d) Y. B. Roh, H. Araki, K. Yoshino, M. Takase, T. Banjyo, *Jpn. J. Appl. Phys., Part 1* **1994**, *33*, 1146-1152; e) M. Piao, M. Wan, F. Lu, *J. Polym. Sci., Part A: Polym. Chem.* **1996**, *34*, 1567-1572; f) P. Bätz, D. Schmeiβer, I. Belaish, D. Davidov, W. Göpel, *Synth. Met.* **1991**, *42*, 1609-1613; g) S. D. Bruck, *Polymer* **1965**, *6*, 319-332; h) A. Bürger, E. Fitzer, M. Heym, B. Terwiesch, *Carbon* **1975**, *13*, 149-157; i) J. I. Gittleman, E. K. Sichel, *J. Electron. Mater.* **1981**, *10*, 327-336.

[6] J. i. Ozaki, S. i. Tanifuji, A. Furuichi, K. Yabutsuka, *Electrochim. Acta* **2010**, *55*, 1864-1871.

[7] R. Srinivasan, R. R. Hall, W. D. Wilson, W. D. Loehle, D. C. Allbee, *Synth. Met.* **1994**, *66*, 301-307.

[8] H. C. Tsai, D. B. Bogy, *J. Vac. Sci. Technol., A* **1987**, *5*, 3287-3312.

[9] T. Amaya, Y. Inada, Y. Shimizu, A. Saeki, R. Tsuji, S. Seki, T. Hirao, *Chem. Asian J.* **2014**, *9*, 2568-2575.

[10] a) T. Ohnishi, I. Murase, T. Noguchi, M. Hirooka, *Synth. Met.* **1987**, *18*, 497-502; b) M. Nakamizo, R. Kammereck, P. L. Walker Jr., *Carbon* **1974**, *12*, 259-267; c) M. Endo, K. Hakamada, C. Kim, N. Miyazawa, T. Kasai, *Tanso* **1998**, *183*, 156-161.

[11] J. I. Inoue, H. Wada, T. Mori, *Jpn. J. Appl. Phys.* **2010**, *49*, 0716051-0716055.

[12] A. C. Ferrari, J. Robertson, *Philos. Trans. R. Soc., A* **2004**, *362*, 2477-2512.

[13] P. Scherrer, *Göttinger Nachrichten Gesell.* **1918**, *2*, 98.

[14] Z. Q. Li, C. J. Lu, Z. P. Xia, Y. Zhou, Z. Luo, *Carbon* **2007**, *45*, 1686-1695.

[15] J. R. Pels, F. Kapteijn, J. A. Moulijn, Q. Zhu, K. M. Thomas, *Carbon* **1995**, *33*, 1641-1653.

[16] T. Amaya, M. Hifumi, M. Okada, Y. Shimizu, T. Moriuchi, K. Segawa, Y. Ando, T. Hirao, *J. Org. Chem.* **2011**, *76*, 8049-8052.

[17] J. F. Moulder, W. F. Stickle, P. E. Sobol, K. D. Bomben, *Handbook of X-ray Photoelectron Spectroscopy*, Perkin-Elmer Corporation, **1992**.

Chapter 3. Energy Threshold of Laser-induced Carbonization in Sumanene Derivatives[4]

3−1. Introduction

The energy threshold of laser-induced carbonization is one of the important factors affecting efficiency of carbonization. Actually, at certain energy of laser employed, some starting materials can be carbonized, while others cannot as described in Chapters 1 and 2. The subsection 2−2−3 in Chapter 2 provided the result that laser-induced carbonization was considered to occur at the relatively low temperature (below ~600 °C), implying that the laser annealing at lower energy was likely to suppress elimination of nitrogen atoms. This finding is expected to provide an important method to synthesize NGCs with retention of N/C ratio.

The procedure to study the energy threshold of laser-induced carbonization consists of the following two processes (Figure 3−1a). The First is laser annealing and the second is check of carbonization through micro-Raman spectroscopy. Recent micro-Raman spectrometers generally equips a laser device as an excitation source. Usage of the laser device that can be worked as a carbonization source enables *in-situ* observation of carbonization utilizing a micro-Raman spectrometer. The *in-situ* observation was utilized in this experiment so as to more effectively perform these two processes in one spectrometer than the conventional technique (Figure 3−1b and c). Even though the literature reported fabrication of carbonous electrodes through laser-induced carbonization and *in-situ* observation of its Raman spectra utilizing a micro-Raman spectroscope, [1]

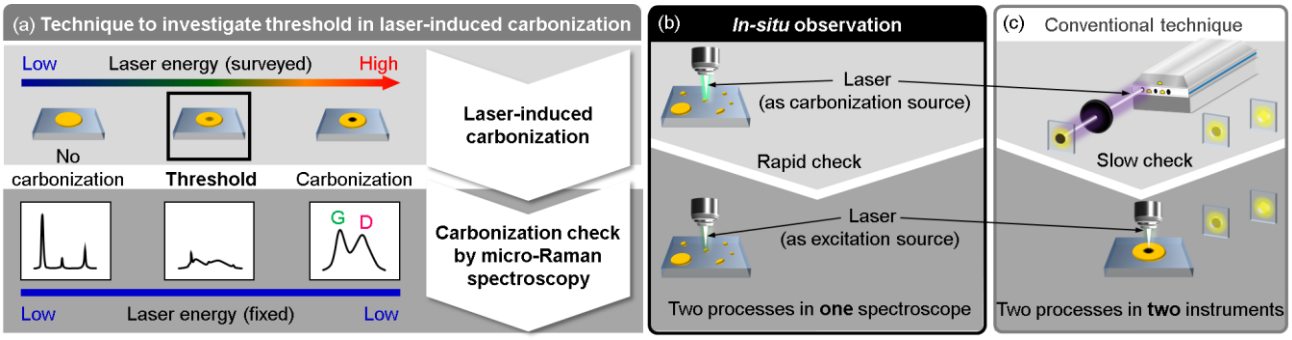

Figure 3−1. Schematic diagram of technique to investigate threshold in laser-induced carbonization. (a) Concept including two processes, laser-induced carbonization and carbonization check by micro-Raman spectroscopy. (b) *In-situ* observation and (c) conventional technique to accomplish the investigation.

there are no reports on the investigation of laser-induced carbonization employing this procedure to the best of the my knowledge.

Based on such background, this chapter focused on the dependence of the energy threshold of laser-induced carbonization on 16 starting materials including sumanene derivatives.

3−2. Results and Discussion

In a micro-Raman spectrometer, the continuous-wave laser (532 nm) was also employed as an annealing source for carbonization by adjusting the laser energy, while the laser was used as an excitation source for Raman measurements. The detection of G and D bands judged whether a sample was carbonized or not (Figure 3−1a). The experiment was carried out under ambient pressure and atmosphere. Figure 3−2 represents the dependence of Raman spectra on laser energy for carbonization in the case when sumanene (**1**), cyclopentaphenanthrene **8**, and fluorene **9** were employed as starting materials. Raman spectra signals after exposing **1** to lower-energy laser (4.1×10^3 and 4.1×10^4 W cm^{-2}) for 1 min were too weak to be clearly observed. As the laser energy for carbonization was increased (7.5×10^4, 1.5×10^5, and 2.9×10^5 W cm^{-2}), G and D bands were clearly detected. The spectrum after laser exposure (2.9×10^5 W cm^{-2}) is similar to that

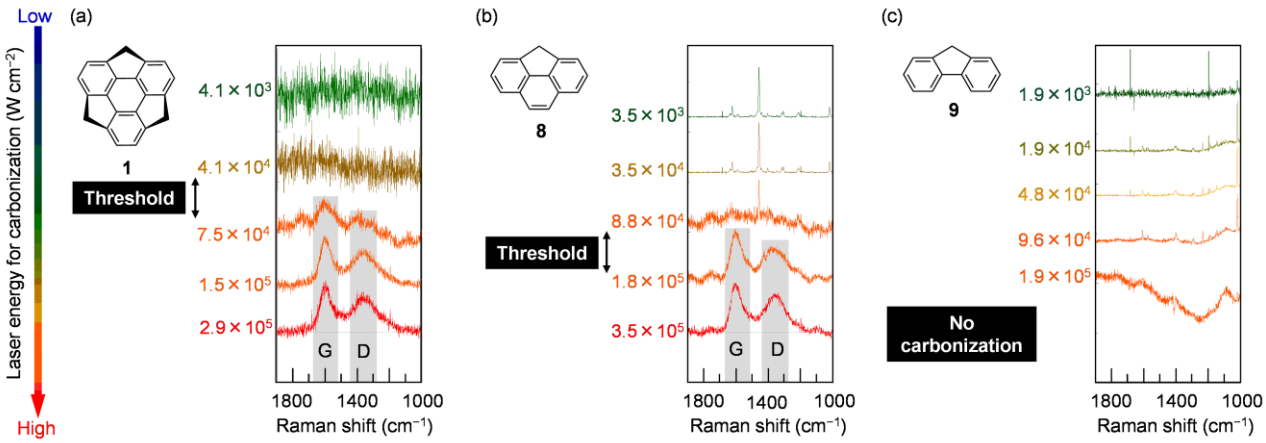

Figure 3−2. Dependence of Raman spectra on 532 nm laser energy for carbonization in (a) **1**, (b) **8**, and (c) **9**. G and D in the graph mean G and D bands, respectively.

formed by heating up to approximately 600−1500 °C.[2] In this case, the range of carbonization energy threshold for **1** is determined as $4.1 \times 10^4 - 7.5 \times 10^4$ W cm^{-2}. On the other hand, in the case of cyclopentaphenanthrene **8**, its intrinsic spectra were seen when the laser energy for carbonization fell below 3.5×10^4 W cm^{-2} (Figure 3−2b). In the next step (8.8×10^4 W cm^{-2}), the intrinsic peaks became disappeared, suggesting that **8** is damaged by the laser exposure. Further enhancement of laser energy (1.8×10^5 and 3.5×10^5 W cm^{-2}) resulted in obvious G and D bands, showing that the threshold exists over range between 8.8×10^4 and 1.8×10^5 W cm^{-2}. Regarding the similar compound **9** (Figure 3−2c), G and D bands were not detected even though the laser worked at a full power (1.9×10^5 W cm^{-2}), where the intrinsic peaks vanished. These results show that the threshold becomes

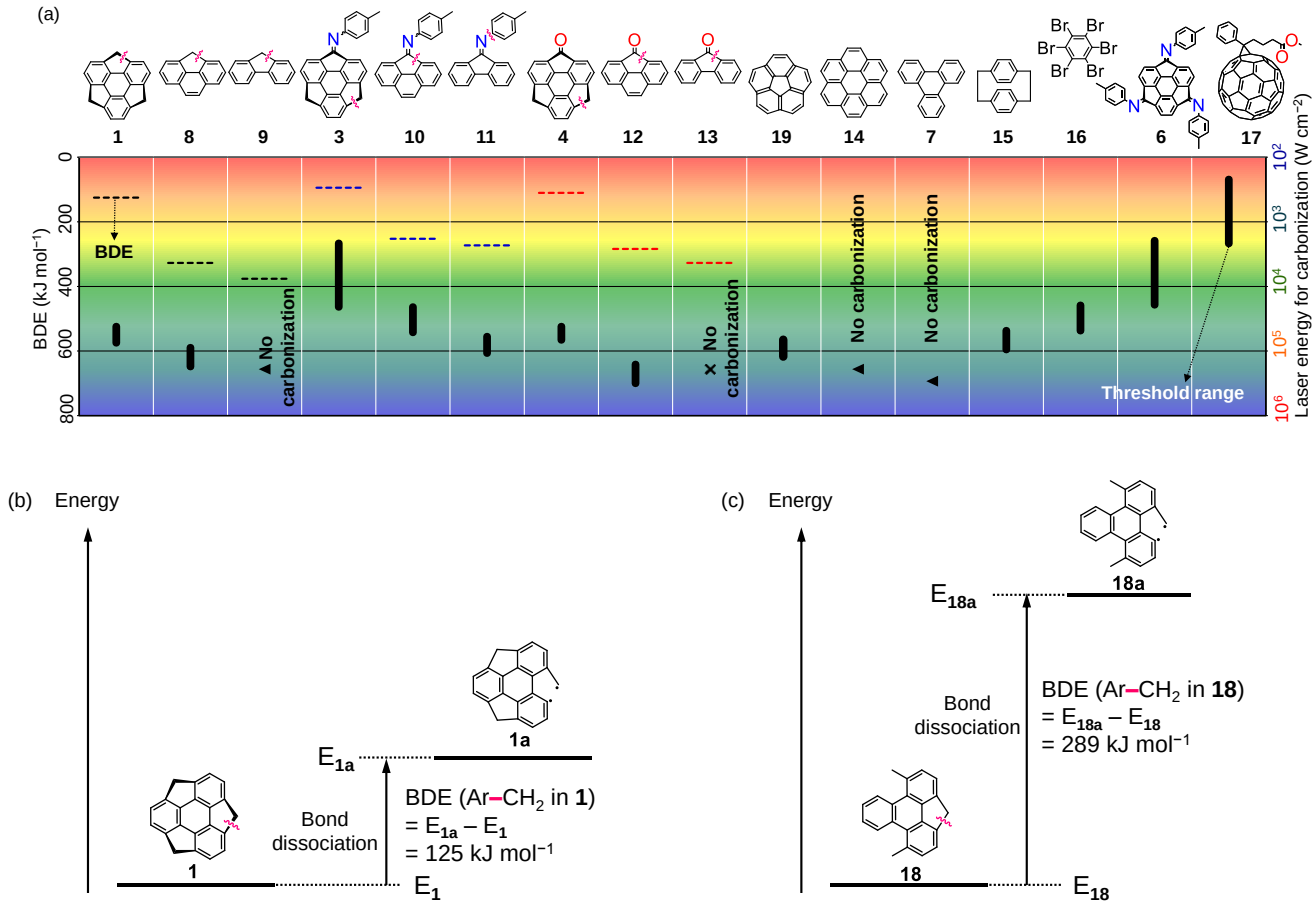

Figure 3−3. (a) Right vertical axis: laser-induced carbonization (532 nm) energy thresholds of **1**, **3**, **4**, **6**−**17** and **19**. Left vertical axis: bond dissociation energies (BDEs) of the weakest bond in **1**, **3**, **4**, **8**−**13**, which are indicated by **~** in their structure formulae. ▬: threshold range, ×: no observation of G and D bands, ◂: difficult to judge whether these bands were observed or not, - - -: BDE. The susceptibility to carbonization increases as the threshold range is shifted to the top. Energy diagrams with bond dissociation of (b) **1** and (c) **18**.

higher in the order of sumanene (**1**) < cyclopentaphenanthrene **8** < fluorene **9**.

Next, the similar experiments were performed for other starting materials. Thus-obtained threshold range are summarized in Figure 3−3a. For non-substituted compounds (**1**, **8**, and **9**), imines (**3**, **10**, and **11**), and ketones (**4**, **12**, and **13**), the threshold was decreased in the following order: fluorene skeleton (**9**, **11**, and **13**) > cyclopentaphenanthrene skeleton (**8**, **10**, and **12**) > sumanene skeleton (**1**, **3**, and **4**) in comparison among the compounds that possess the identical substituent. This order is in accordance with increase of the lowest bond dissociation energy (BDE) among the bonds included in each compound, where the lowest BDE was estimated by the density functional theory (DFT) calculation [non-substituted compounds (**9**: 376 > **8**: 327 > **1**: 125 kJ mol^{-1}), imines (**11**: 273 > **10**: 253 > **3**: 95 kJ mol^{-1}), ketones (**13**: 327 > **12**: 284 > **4**: 111 kJ mol^{-1})] (Figure 3−3a). The BDE in sumanene (**1**) is much lower than the other skeletons, which is considered to be caused by release of strain energy inherent in it on the occasion of the bond dissociation. This can be understood from the results that the BDE in sumanene (**1**, 125 kJ mol^{-1}, Figure 3−3b) was much lower than that in model planar molecule **18** (289 kJ mol^{-1}, Figure 3−3c).

Light absorption efficiency is also considered to affect the threshold. In fact, while these compounds have virtually no light absorption at 532 nm at least in a solution state,[3] it is suggested that they absorb the 532 nm light in a solid state and/or that multiphoton absorption[4] occurs.

The carbonization was not observed for coronene (**14**) and triphenylene (**7**) through laser annealing at maximum energy ($1.9 – 2.9 \times 10^5$ W cm^{-2}). In contrast, corannulene (**19**) was carbonized with the threshold range ($7.4 \times 10^4 – 1.3 \times 10^5$ W cm^{-2}), which is similar to that for sumanene. From the aspect of the BDE, it is assumed that the BDE in **19** should be higher than that in **1** because **19** possesses less strain than that in **1** (the bowl depth is 0.89 Å[5] for **19** and 1.11 Å[6] for **1**) and only sp^2 bonds, whose BDE is generally higher than that of only sp^3 bonds. This is potentially due to the light absorption efficiency and/or strain of corannulene skeleton.

Moreover, [2.2]paracyclophane (**15**), which bears four methylene carbons, was employed. Its carbonization was observed at the laser energy of 1.9×10^5 W cm^{-2}. In the case of hexabromobenzene (**16**), having the weaker bonds, carbonization occurred under less laser-energy conditions (4.9×10^4 W cm^{-2}) than that for **6**. Sumanenetrione triimine **6**, which bears the more imino groups than sumanenemonoone imine **3**, showed the

similar threshold range as that of **3**. These findings suggest that the reaction involving the laser annealing might proceed, once one bond is dissociated regardless of the number of substituent groups. Finally, [6,6]-phenyl-C_{61}-butyric acid methyl ester (PCBM, **17**) was tested as well to result in the lower threshold range ($2.2 \times 10^2 – 2.2 \times 10^3$ W cm^{-2}) than the other compounds employed in the experiments. This might be due to the reason such as an inherent large strain and/or a good absorption of visible light[7] in the fullerene derivative.

3−3. Conclusion

In summary, this chapter revealed that the energy threshold of the laser-induced carbonization (532 nm, CW) decreased in the following order: fluorene skeleton > cyclopentaphenanthrene skeleton > sumanene skeleton, suggesting they became susceptible in this order. Moreover, PCBM (**17**) was more susceptible than bowl-shaped molecule (**1**, **3**, **4**, **6**, and **19**) and planar molecule (**8**–**13**), while coronene (**14**) and triphenylene (**7**) were difficult to be carbonized under the laser parameters employed.

3−4. Experimental Section

General Method

^{1}H (400 MHz) and ^{13}C (100 MHz) NMR spectra were measured on a JEOL JNM-ECS 400 spectrometer. $CDCl_3$ was employed as a solvent. The residual $CHCl_3$ peak (δ= 7.26 or 77.0) was used as references for ^{1}H or ^{13}C NMR, respectively. Infrared spectra were recorded on a JASCO FT/IR-480plus. Mass spectra were measured on a BRUKER AUTOFLEX III (MALDI−TOF) mass spectrometer. Reagents were purchased from commercial sources and used without further purification unless otherwise indicated.

Materials

The compounds **1**, **3**, **4**, **6**−**17**, and **19** were employed in the experiments. Among them, **7**−**9**, **13**−**17**, and **19** were purchased from commercial sources and used without further purification. The compounds **1**,[8] **4**,[9] and

11[10] were synthesized according to the procedures reported previously. Synthesis of **3** and **6** was described in Chapter 1 and Chapter 2, respectively. The other compounds **10**−**12** used were synthesized according to the following procedures.

Synthesis

4*H*-cyclopenta[*def*]phenanthren-4-one (12)

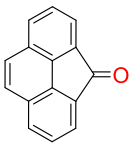

12

A round-bottomed flask equipped with a magnetic stirring bar was charged with 4*H*-cyclopenta[*def*]phenanthrene (**8**) (72.1 mg, 0.379 mmol), ruthenium(III) chloride hydrate (133.4 mg), pyridine (5 mL), and dichloromethane (20 mL). To the stirred reaction mixture was added *t*-butyl hydroperoxide solution (70% in H_2O, 1.0 mL) at room temperature. After stirring at room temperature for 4 days, the reaction was quenched by addition of a solution mixture (~4 mL) [aqueous $Na_2S_2O_3$ water (32 wt%)/saturated aqueous $NaHCO_3$ water = 1/2 (volume ratio)]. The reaction mixture was poured into desalted water and dichloromethane. The aqueous layer was extracted twice with dichloromethane. The combined organic layer was washed with 1N HCl aqueous solution (twice), brine, dried over Na_2SO_4, and evaporated *in vacuo*. The residue was purified through a short pad of silica gel (height: ~3 cm) with dichloromethane to afford the crude product (69.4 mg). The product was purified by reprecipitation (dichloromethane/methanol). After gathering the precipitated yellow solid of **12** (17.0 mg), a filtrate was recovered. From the filtrate, the reprecipitation was performed again, and then **12** (11.7 mg) was separated from a filtrate. Using the filtrate, further recrystallization (dichloromethane/methanol = 1/8) was carried out to yield **12** as a yellow solid (15.0 mg). These purifications gave the pure desired compound **12** (43.7 mg in total, 0.214 mmol, 56% yield): ^{1}H NMR (400 MHz, $CDCl_3$): δ =7.90 (dd, J = 8.0, 0.4 Hz, 2H), 7.79 (dd, J = 7.0, 0.4 Hz, 2H), 7.77 (s, 2H), 7.58 (dd, J = 8.0, 7.0 Hz, 2H) ppm [lit.,[11] ($CDCl_3$): δ = 7.82 (dd, J = 7.5, 1.4 Hz, 2H), 7.72 (dd, J = 6.8, 1.4 Hz, 2H), 7.67 (s, 2H), 7.45 (dd, J = 7.5, 6.8 Hz, 2H) ppm]. The slight difference between the chemical shifts of our sample and reported ones are

considered to arise from the concentration difference as one possibility.

***N*-(*p*-tolyl)-4*H*-cyclopenta[*def*]phenanthren-4-imine (10)**

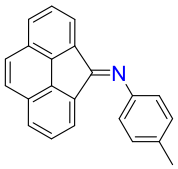

10

A dried reaction apparatus purged with nitrogen was equipped with reflux condenser, dried 20 mL two-necked flask set with a magnetic stirring bar, and a solvent reservoir where an activated MS4A (pellet, 5.0 g) was put (see diagram below). After the flask was charged with 4*H*-cyclopenta[*def*]phenanthren-4-one (**12**) (15.0 mg, 0.0734 mmol), *p*–toluidine (63.0 mg, 0.588 mmol, 8 eq.), and anhydrous toluene (10 mL), the mixture was stirred and heated up to 130 °C. During the reaction, the following operation was repeated several times: once the solvent entirely evaporated out through path 1, the solvent in the reservoir was returned to the flask from path 2 through the MS4A by opening the cock 1. In the first 90 min, this operation was repeated each 30 min. In the next 80 min, this operation was repeated each 10 min, where further *p*-toluidine (63.0 mg, 0.588 mmol, 8 eq.) was added in the fifth operation. In the final 60 min, this operation was repeated each 30 min. After that, the reaction mixture was evaporated *in vacuo* to give the crude product as a yellow solid (21.7 mg, 95% conversion). The residue was purified by preparative thin-layer chromatography (hexane/dichloromethane = 1/1) to afford **10** (18.7 mg, 3% impurity) as a yellow solid. Further purification was undertaken by preparative thin-layer chromatography (hexane/ethyl acetate = 2/1) to provide **10** (including 1% **12**) as a yellow solid. Finally, the solid was refined by recrystallization (hexane/dichloromethane, cooling from 25 °C to −7 °C at the rate of 0.1 °C min^{-1}) to yield the target compound **10** (4.2 mg, 0.0143 mmol, including 1% **12**) as needle-like yellow crystals: FT−IR (ATR, powder): ν = 3053, 2918, 2855, 1621, 1504 cm^{-1}; ^{1}H NMR (400 MHz, $CDCl_3$): δ = 8.02 (d, J = 7.1 Hz, 1H), 7.89 (d, J = 8.0 Hz,

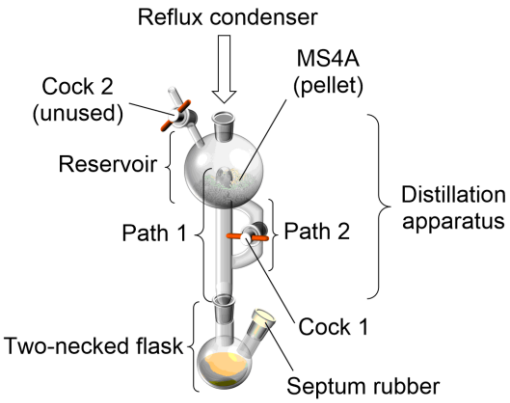

1H), 7.82−7.71 (m, 3H), 7.66 (m, 1H), 7.30−7.24 (m, 3H), 7.03 (d, *J* = 8.0 Hz, 2H), 6.74 (d, *J* = 7.3 Hz, 1H), 2.46 (s, 3H) ppm; ^{13}C NMR (100 MHz, $CDCl_3$): δ = 164.61, 149.28, 138.46, 137.78, 136.21, 134.26, 130.48, 130.00, 128.78, 128.13, 128.10, 127.77, 127.65, 127.43, 125.35, 124.97, 121.08, 119.00, 21.23 ppm (because these results lack one peak, two peaks are considered to be accidentally coincident.); HRMS (MALDI−TOF): *m*/*z* calcd for $C_{22}H_{15}N$ [M^+] 293.1199, found 293.1188.

Investigation of Energy Threshold in Laser-induced Carbonization Using a Micro-Raman Spectroscope

Sample preparation

Each compound (~1 mg) was generally dissolved with 100 μL of dichloromethane (toluene was used for **17**). The solution (~5 μL) was dropcasted onto a glass substrate. After drying in air, it was further dried *in vacuo*. The solvents were commercially available and employed without further purification.

Carbonization and Raman measurements

To investigate the energy threshold in laser-induced carbonization of the above-mentioned samples, green continuous-wave (CW) laser (532 nm) equipped in a micro-Raman spectrometer (JASCO, NRS−3100) was utilized not only as exciting source for Raman measurements but also as heat source for carbonization. The laser energy can be monitored anytime and stepwise controlled through a neutral density (ND) filter with optical density (OD) of 3, 2, 1, 0.6, and 0.3, which can be manually switched by the software. In the case when an ND filter was not inserted, the value of OD was represented as 0. The laser output energy depends on ambient conditions. The laser beam can be focused through an objective lens (20 or 100 times), where the beam diameter was ~4 or ~1 μm, respectively.

First of all, the each sample was mounted onto the stage of the micro spectrometer. A lot of particles with various sizes were observed through its microscope in each sample. Note that the particle size chosen for the measurement should be similar in size to the laser beam diameter because it affects the spectrum after exposing the sample to laser. In fact, in the case of a too large particle, the signal derived from a carbonized region was buried within that of an intrinsic region. In contrast, in the case of a too small particle, the signal was too small

to be detected. Especially when a sample employed emits fluorescence resulted from excitation by laser, attention to choose a particle should be paid not so as to bury the signal obtained from a carbonized region within that of the fluorescence.

Secondary, the each sample was exposed to laser under the conditions for carbonization as shown in Tables E3−1 ~ E3−16. Then, the spectra after laser exposure were taken under conditions for Raman measurement as listed in Tables E3−1 ~ E3−16. The laser energy for the measurements was cared not so as to exceed that for carbonization. The raw spectra were modified by subtracting linear background and normalizing them in order to easily find G and D bands (~1600 and ~1360 cm^{-1}, respectively) and compare them with each other. The modification was undertaken using an analysis software (JASCO, Spectra Manager Version 2).

Thirdly, the judgment was performed regarding whether G and D bands were detected or not. The results are listed in Tables E3−1 ~ E3−16, where the denotations ×, ▲, and ○ were used in the case when G and D bands were not detected, when it was difficult to judge detection of G and D bands, and when G and D bands were clearly detected, respectively.

Finally, the carbonization energy threshold was determined as the range of the laser energy corresponding to the region between ▲ and ○ or between × and ○.

Table E3−1. Carbonization and Raman measurement conditions, and the resulting raw and modified Raman spectra after exposing **1** to 532 nm laser.

1

Carbonization conditions[a]			Raman measurment conditions[a]				Specra after laser exposure		
OD[b]	Laser energy (W cm^{-2})	Exposure time (s)	OD[b]	Laser energy (W cm^{-2})	Exposure time (s)	Cumulative number	Raw	Modified[c]	G and D bands[d]
2	4.1×10^{3}	60	2	4.1×10^{3}	5	5	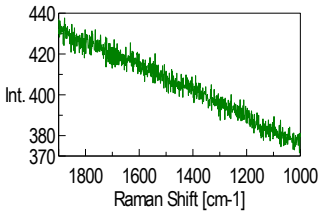	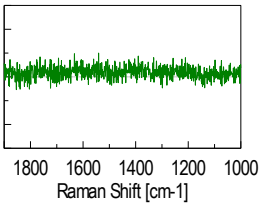	×
1	4.1×10^{4}	60	2	4.1×10^{3}	5	5	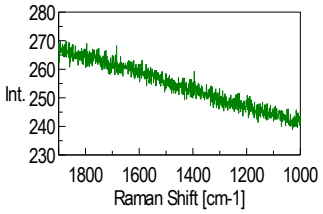	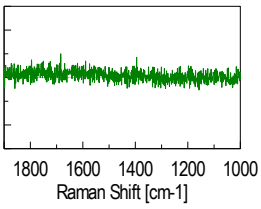	×
0.6	7.5×10^{4}	30	2	4.1×10^{3}	5	5	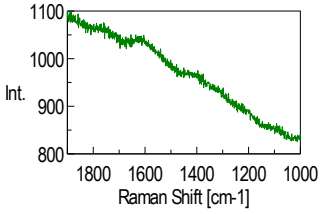	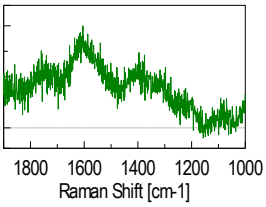	○
0.3	1.5×10^{5}	10	2	4.1×10^{3}	5	5	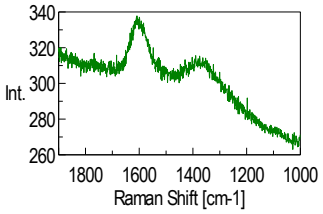	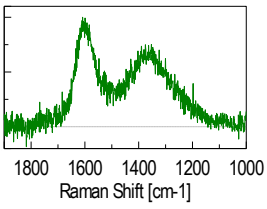	○
0	2.9×10^{5}	5	2	4.1×10^{3}	5	5	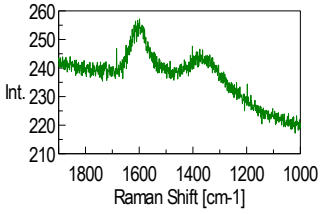	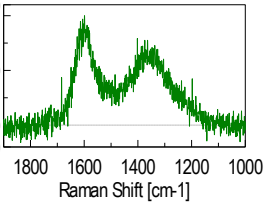	○

[a] Magnification of objective lens was 100 times.

[b] Optical density (OD) of a neutral density (ND) filter.

[c] Modified spectra were displayed after subtracting linear background and normalizing them for ease of comparing them with each other. Vertical axis exhibits the Raman intensity with arbitrary unit.

[d] ×, ▲, and ○ denote the case when G and D bands were not detected, when it was difficult to judge detection of G and D bands, and when G and D bands were clearly detected, respectively.

Table E3−2. Carbonization and Raman measurement conditions, and the resulting raw and modified Raman spectra after exposing **8** to 532 nm laser.

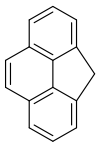

8

Carbonization conditions[a]			Raman measurment conditions[a]				Specra after laser exposure		
OD[b]	Laser energy (W cm^{-2})	Exposure time (s)	OD[b]	Laser energy (W cm^{-2})	Exposure time (s)	Cumulative number	Raw	Modified[c]	G and D bands[d]
2	3.5×10^{3}	30	3	3.5×10^{2}	5	10	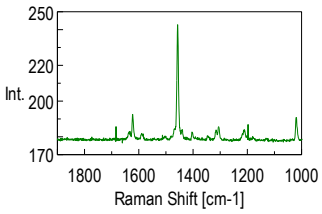	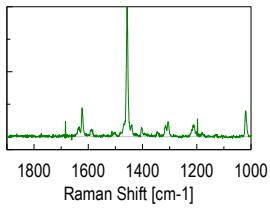	×
1	3.5×10^{4}	30	3	3.5×10^{2}	5	10	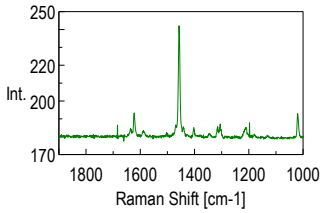	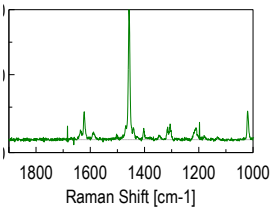	×
0.6	8.8×10^{4}	60	3	3.5×10^{2}	5	10	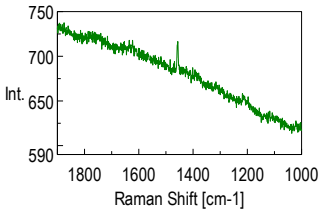	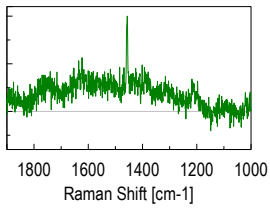	▲
0.3	1.8×10^{5}	60	1	3.5×10^{2}	5	10	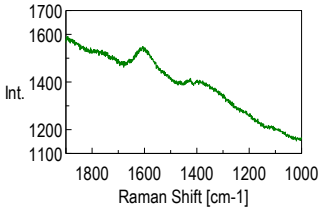	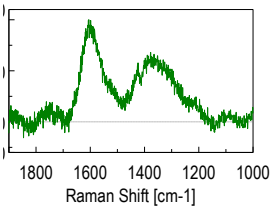	○
0	3.5×10^{5}	120	1	3.5×10^{2}	5	10	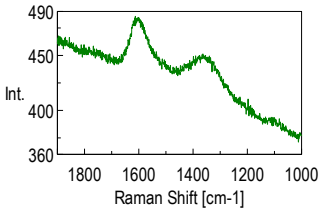	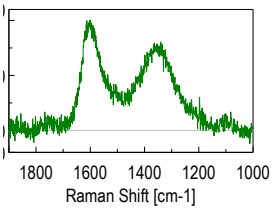	○

[a] Magnification of objective lens was 100 times.

[b] Optical density (OD) of a neutral density (ND) filter.

[c] Modified spectra were displayed after subtracting linear background and normalizing them for ease of comparing them with each other. Vertical axis exhibits the Raman intensity with arbitrary unit.

[d] ×, ▲, and ○ denote the case when G and D bands were not detected, when it was difficult to judge detection of G and D bands, and when G and D bands were clearly detected, respectively.

Table E3−3. Carbonization and Raman measurement conditions, and the resulting raw and modified Raman spectra after exposing **9** to 532 nm laser.

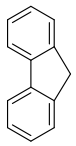

9

Carbonization conditions[a]			Raman measurment conditions[a]				Specra after laser exposure		
OD[b]	Laser energy (W cm^{-2})	Exposure time (s)	OD[b]	Laser energy (W cm^{-2})	Exposure time (s)	Cumulative number	Raw	Modified[c]	G and D bands[d]
2	1.9×10^{3}	60	2	1.9×10^{3}	5	20	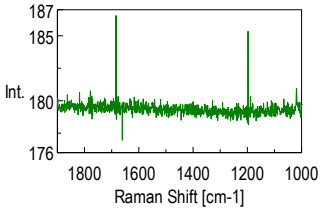	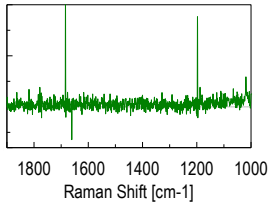	×
1	1.9×10^{4}	60	1	1.9×10^{4}	5	20	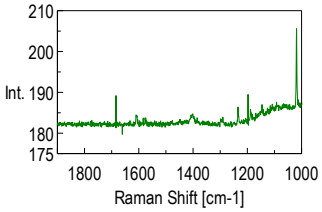	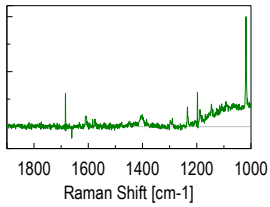	×
0.6	4.8×10^{4}	60	0.6	4.8×10^{4}	5	20	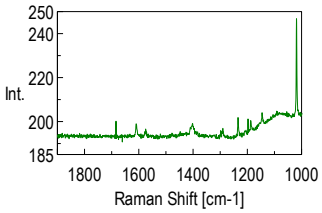	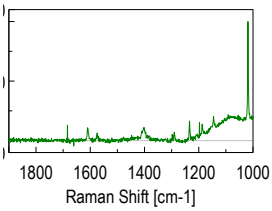	×
0.3	9.6×10^{4}	60	0.3	9.6×10^{4}	5	20	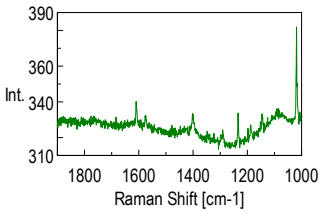	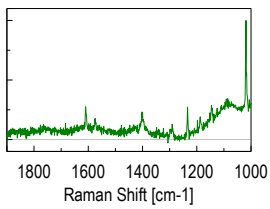	×
0	1.9×10^{5}	60	0	1.9×10^{5}	60	20	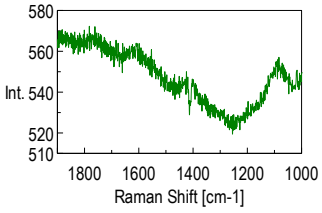	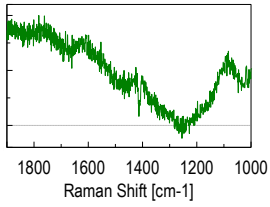	▲

[a] Magnification of objective lens was 100 times.

[b] Optical density (OD) of a neutral density (ND) filter.

[c] Modified spectra were displayed after subtracting linear background and normalizing them for ease of comparing them with each other. Vertical axis exhibits the Raman intensity with arbitrary unit.

[d] ×, ▲, and ○ denote the case when G and D bands were not detected, when it was difficult to judge detection of G and D bands, and when G and D bands were clearly detected, respectively.

Table E3−4. Carbonization and Raman measurement conditions, and the resulting raw and modified Raman spectra after exposing **3** to 532 nm laser.

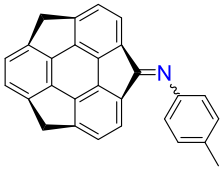

3

Carbonization conditions[a]			Raman measurment conditions[a]				Specra after laser exposure		
OD[b]	Laser energy (W cm^{-2})	Exposure time (s)	OD[b]	Laser energy (W cm^{-2})	Exposure time (s)	Cumulative number	Raw	Modified[c]	G and D bands[d]
2	2.1×10^{3}	60	2	2.1×10^{3}	5	20	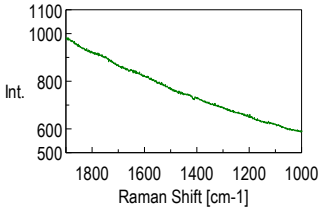	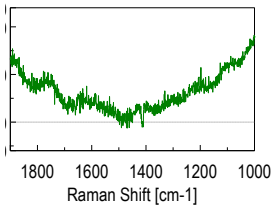	▲
1	2.1×10^{4}	60	2	2.1×10^{3}	5	20	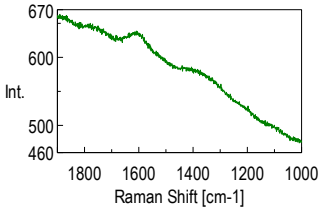	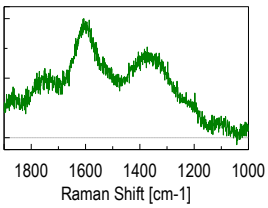	○
0.6	5.3×10^{4}	60	2	2.1×10^{3}	5	20	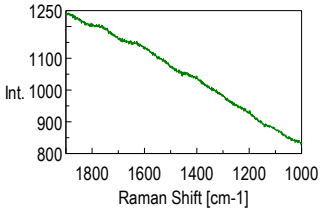	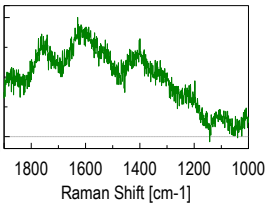	○
0.3	1.0×10^{5}	60	2	2.1×10^{3}	5	20	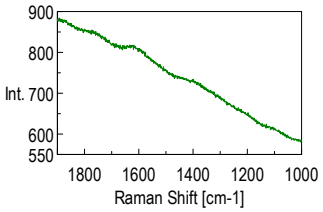	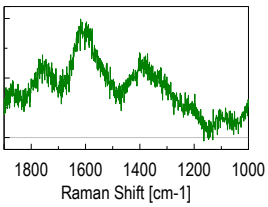	○
0	2.1×10^{5}	60	2	2.1×10^{3}	5	20	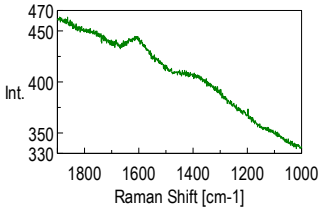	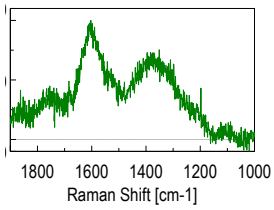	○

[a] Magnification of objective lens was 100 times.

[b] Optical density (OD) of a neutral density (ND) filter.

[c] Modified spectra were displayed after subtracting linear background and normalizing them for ease of comparing them with each other. Vertical axis exhibits the Raman intensity with arbitrary unit.

[d] ×, ▲, and ○ denote the case when G and D bands were not detected, when it was difficult to judge detection of G and D bands, and when G and D bands were clearly detected, respectively.

Table E3−5. Carbonization and Raman measurement conditions, and the resulting raw and modified Raman spectra after exposing **10** to 532 nm laser.

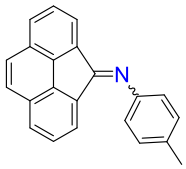

10

Carbonization conditions[a]			Raman measurment conditions[a]				Specra after laser exposure		
OD[b]	Laser energy (W cm^{-2})	Exposure time (s)	OD[b]	Laser energy (W cm^{-2})	Exposure time (s)	Cumulative number	Raw	Modified[c]	G and D bands[d]
3	2.0×10^{2}	60	2	2.0×10^{3}	5	20	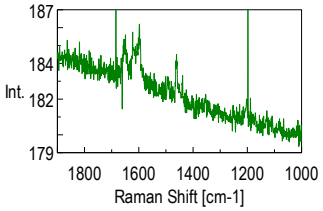	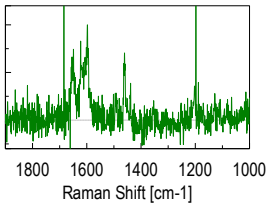	×
2	2.0×10^{3}	60	2	2.0×10^{3}	5	20	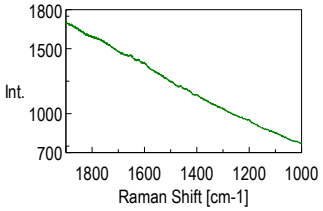	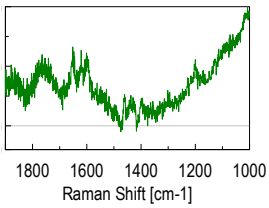	×
1	2.1×10^{4}	60	2	2.0×10^{3}	5	20	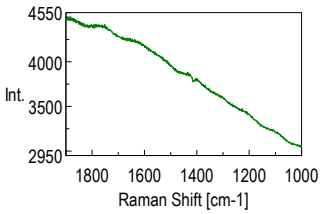	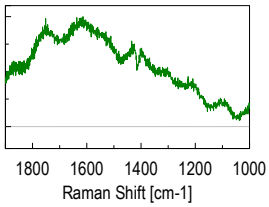	▲
0.6	5.2×10^{4}	60	2	2.0×10^{3}	5	20	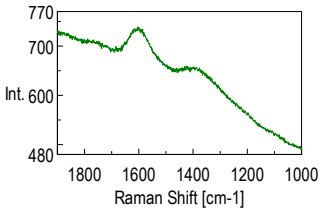	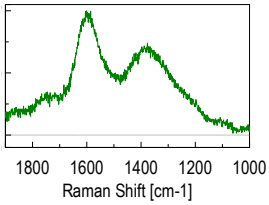	○
0.3	1.0×10^{5}	60	2	2.0×10^{3}	5	20	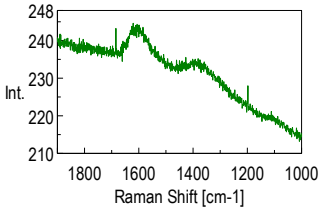	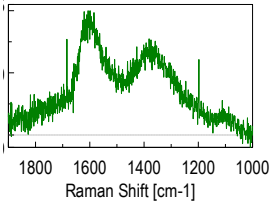	○

[a] Magnification of objective lens was 100 times.

[b] Optical density (OD) of a neutral density (ND) filter.

[c] Modified spectra were displayed after subtracting linear background and normalizing them for ease of comparing them with each other. Vertical axis exhibits the Raman intensity with arbitrary unit.

[d] ×, ▲, and ○ denote the case when G and D bands were not detected, when it was difficult to judge detection of G and D bands, and when G and D bands were clearly detected, respectively.

Table E3−6. Carbonization and Raman measurement conditions, and the resulting raw and modified Raman spectra after exposing **11** to 532 nm laser.

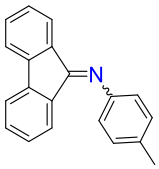

11

Carbonization conditions[a]			Raman measurment conditions[a]				Specra after laser exposure		
OD[b]	Laser energy (W cm^{-2})	Exposure time (s)	OD[b]	Laser energy (W cm^{-2})	Exposure time (s)	Cumulative number	Raw	Modified[c]	G and D bands[d]
2	2.2×10^{3}	60	2	2.2×10^{3}	5	20	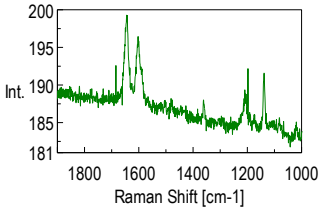	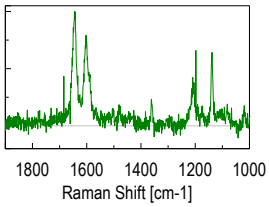	×
1	2.2×10^{4}	60	2	2.2×10^{3}	5	20	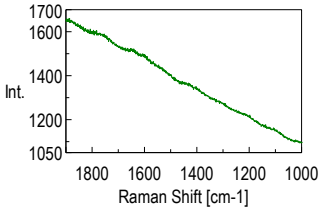	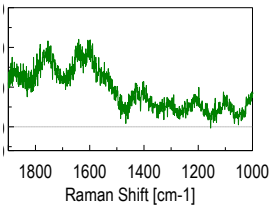	▲
0.6	5.9×10^{4}	60	2	2.2×10^{3}	5	20	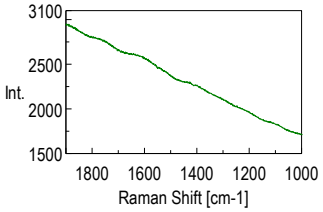	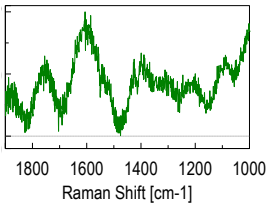	▲
0.3	1.1×10^{5}	60	2	2.2×10^{3}	5	20	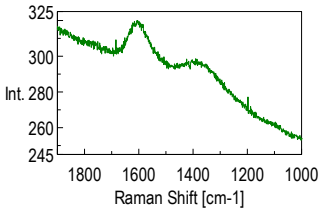	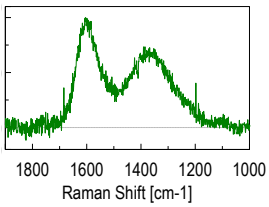	○
0	2.2×10^{5}	60	2	2.2×10^{3}	5	20	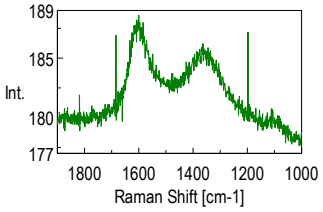	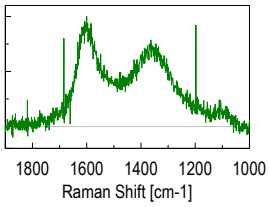	○

[a] Magnification of objective lens was 100 times.

[b] Optical density (OD) of a neutral density (ND) filter.

[c] Modified spectra were displayed after subtracting linear background and normalizing them for ease of comparing them with each other. Vertical axis exhibits the Raman intensity with arbitrary unit.

[d] ×, ▲, and ○ denote the case when G and D bands were not detected, when it was difficult to judge detection of G and D bands, and when G and D bands were clearly detected, respectively.

Table E3−7. Carbonization and Raman measurement conditions, and the resulting raw and modified Raman spectra after exposing **4** to 532 nm laser.

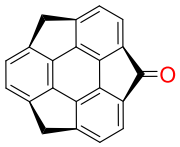

4

Carbonization conditions[a]			Raman measurment conditions[a]				Specra after laser exposure		
OD[b]	Laser energy (W cm^{-2})	Exposure time (s)	OD[b]	Laser energy (W cm^{-2})	Exposure time (s)	Cumulative number	Raw	Modified[c]	G and D bands[d]
2	2.9×10^{3}	60	2	2.9×10^{3}	5	5	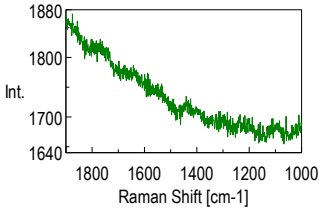	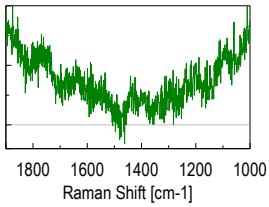	▲
1	4.1×10^{4}	60	2	2.9×10^{3}	5	5	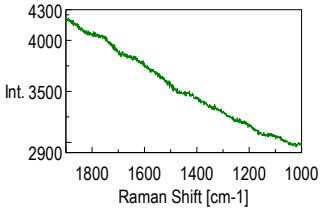	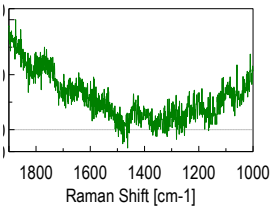	▲
0.6	6.8×10^{4}	60	2	2.9×10^{3}	5	5	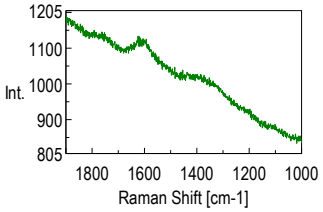	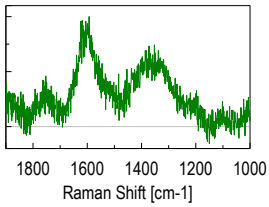	○
0.3	1.5×10^{5}	60	2	2.9×10^{3}	5	5	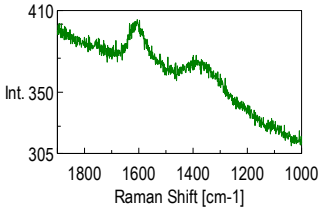	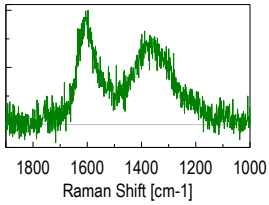	○
0	2.9×10^{5}	60	2	2.9×10^{3}	5	5	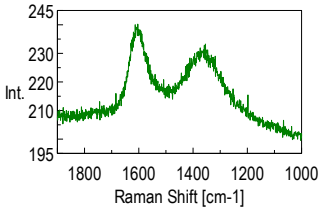	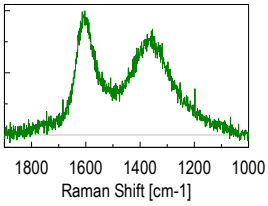	○

[a] Magnification of objective lens was 100 times.

[b] Optical density (OD) of a neutral density (ND) filter.

[c] Modified spectra were displayed after subtracting linear background and normalizing them for ease of comparing them with each other. Vertical axis exhibits the Raman intensity with arbitrary unit.

[d] ×, ▲, and ○ denote the case when G and D bands were not detected, when it was difficult to judge detection of G and D bands, and when G and D bands were clearly detected, respectively.

Table E3−8. Carbonization and Raman measurement conditions, and the resulting raw and modified Raman spectra after exposing **12** to 532 nm laser.

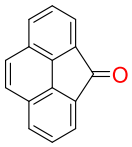

12

Carbonization conditions[a]			Raman measurment conditions[a]				Specra after laser exposure		
OD[b]	Laser energy (W cm^{-2})	Exposure time (s)	OD[b]	Laser energy (W cm^{-2})	Exposure time (s)	Cumulative number	Raw	Modified[c]	G and D bands[d]
2	3.2×10^{3}	60	2	3.2×10^{3}	5	10	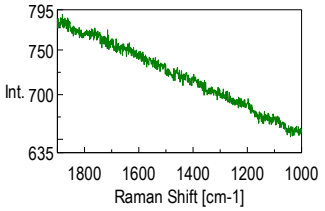	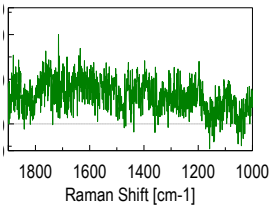	×
1	3.2×10^{4}	60	2	3.2×10^{3}	5	10	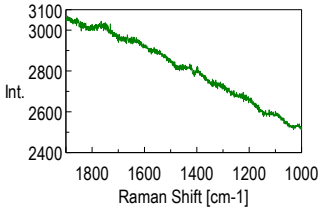	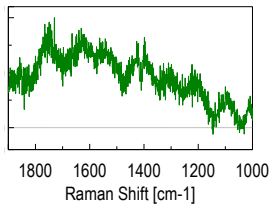	▲
0.6	8.0×10^{4}	60	2	3.2×10^{3}	5	10	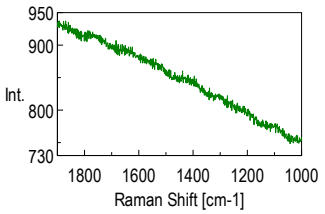	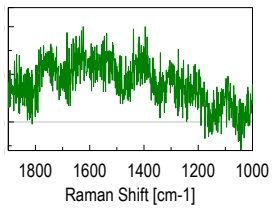	▲
0.3	1.6×10^{5}	60	2	3.2×10^{3}	5	10	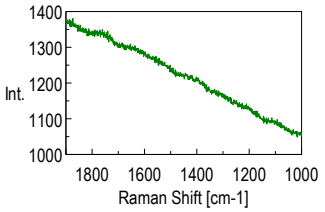	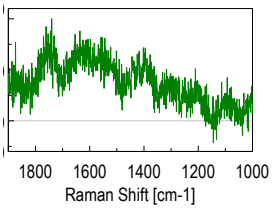	▲
0	3.2×10^{5}	60	2	3.2×10^{3}	5	20	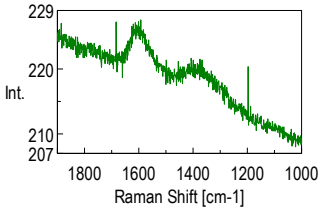	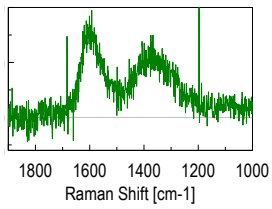	○

[a] Magnification of objective lens was 100 times.

[b] Optical density (OD) of a neutral density (ND) filter.

[c] Modified spectra were displayed after subtracting linear background and normalizing them for ease of comparing them with each other. Vertical axis exhibits the Raman intensity with arbitrary unit.

[d] ×, ▲, and ○ denote the case when G and D bands were not detected, when it was difficult to judge detection of G and D bands, and when G and D bands were clearly detected, respectively.

Table E3−9. Carbonization and Raman measurement conditions, and the resulting raw and modified Raman spectra after exposing **13** to 532 nm laser.

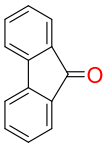

13

Carbonization conditions[a]			Raman measurment conditions[a]				Specra after laser exposure		
OD[b]	Laser energy (W cm^{-2})	Exposure time (s)	OD[b]	Laser energy (W cm^{-2})	Exposure time (s)	Cumulative number	Raw	Modified[c]	G and D bands[d]
2	1.9×10^{3}	60	2	1.9×10^{3}	5	20	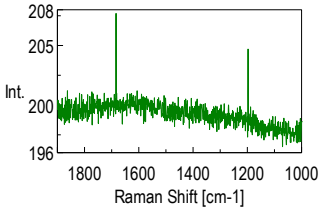	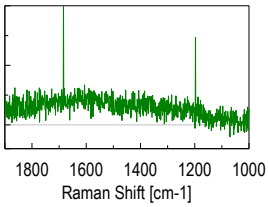	×
1	1.9×10^{4}	60	1	1.9×10^{4}	5	20	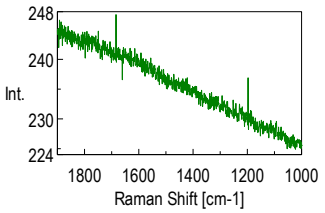	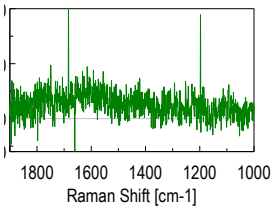	×
0.6	5.0×10^{4}	60	0.6	5.0×10^{4}	5	20	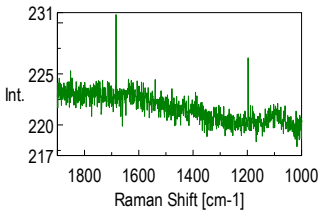	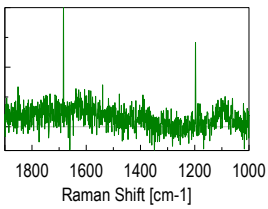	×
0.3	9.7×10^{4}	60	0.3	9.7×10^{4}	5	20	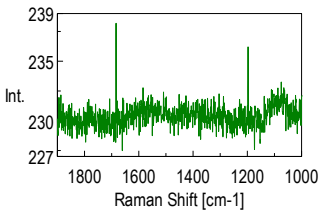	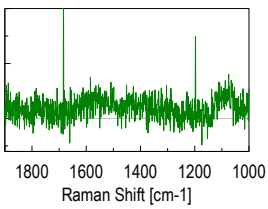	×
0	1.9×10^{5}	60	0	1.9×10^{5}	5	20	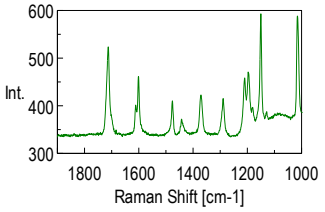	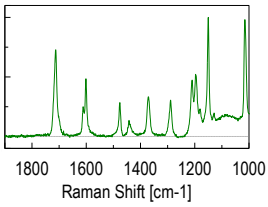	×

[a] Magnification of objective lens was 100 times.

[b] Optical density (OD) of a neutral density (ND) filter.

[c] Modified spectra were displayed after subtracting linear background and normalizing them for ease of comparing them with each other. Vertical axis exhibits the Raman intensity with arbitrary unit.

[d] ×, ▲, and ○ denote the case when G and D bands were not detected, when it was difficult to judge detection of G and D bands, and when G and D bands were clearly detected, respectively.

Table E3−10. Carbonization and Raman measurement conditions, and the resulting raw and modified Raman spectra after exposing **19** to 532 nm laser.

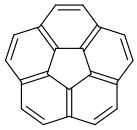

19

Carbonization conditions[a]			Raman measurment conditions[a]				Specra after laser exposure		
OD[b]	Laser energy (W cm^{-2})	Exposure time (s)	OD[b]	Laser energy (W cm^{-2})	Exposure time (s)	Cumulative number	Raw	Modified[c]	G and D bands[d]
2	2.7×10^{3}	60	2	2.7×10^{3}	5	10	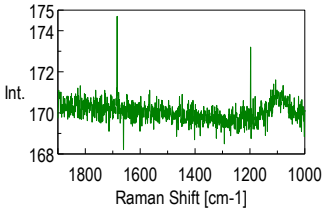	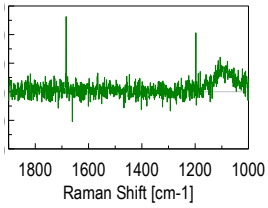	×
1	2.7×10^{4}	15	1	2.7×10^{4}	5	10	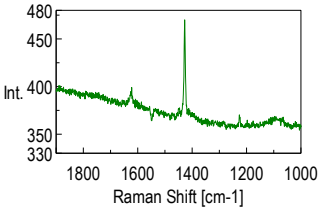	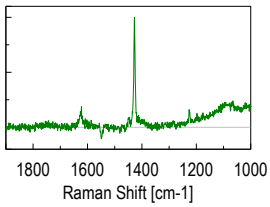	×
0.6	7.4×10^{4}	60	1	2.5×10^{4}	5	10	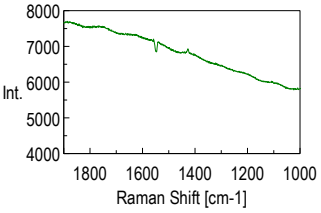	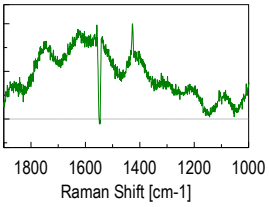	▲
0.3	1.3×10^{5}	20	1	2.6×10^{4}	5	10	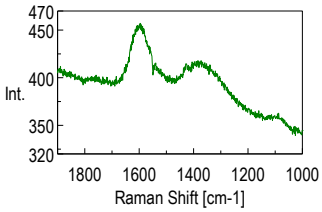	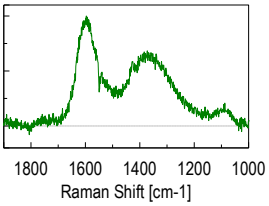	○

[a] Magnification of objective lens was 100 times.

[b] Optical density (OD) of a neutral density (ND) filter.

[c] Modified spectra were displayed after subtracting linear background and normalizing them for ease of comparing them with each other. Vertical axis exhibits the Raman intensity with arbitrary unit.

[d] ×, ▲, and ○ denote the case when G and D bands were not detected, when it was difficult to judge detection of G and D bands, and when G and D bands were clearly detected, respectively.

Table E3−11. Carbonization and Raman measurement conditions, and the resulting raw and modified Raman spectra after exposing **14** to 532 nm laser.

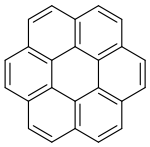

14

Carbonization conditions[a]			Raman measurment conditions[a]				Specra after laser exposure		
OD[b]	Laser energy (W cm^{-2})	Exposure time (s)	OD[b]	Laser energy (W cm^{-2})	Exposure time (s)	Cumulative number	Raw	Modified[c]	G and D bands[d]
0	1.9×10^{5}	60	0	1.9×10^{5}	1	20	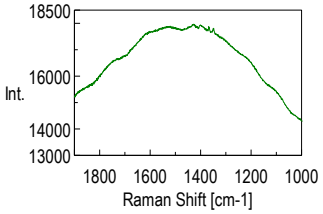	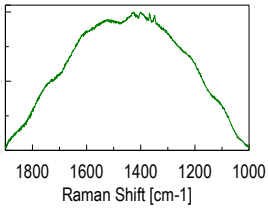	▲

[a] Magnification of objective lens was 100 times.

[b] Optical density (OD) of a neutral density (ND) filter.

[c] Modified spectra were displayed after subtracting linear background and normalizing them for ease of comparing them with each other. Vertical axis exhibits the Raman intensity with arbitrary unit.

[d] ×, ▲, and ○ denote the case when G and D bands were not detected, when it was difficult to judge detection of G and D bands, and when G and D bands were clearly detected, respectively.

Table E3−12. Carbonization and Raman measurement conditions, and the resulting raw and modified Raman spectra after exposing **5** to 532 nm laser.

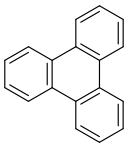

7

Carbonization conditions[a]			Raman measurment conditions[a]				Specra after laser exposure		
OD[b]	Laser energy (W cm^{-2})	Exposure time (s)	OD[b]	Laser energy (W cm^{-2})	Exposure time (s)	Cumulative number	Raw	Modified[c]	G and D bands[d]
2	3.8×10^{3}	5	2	3.8×10^{3}	5	20	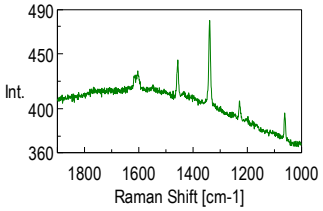	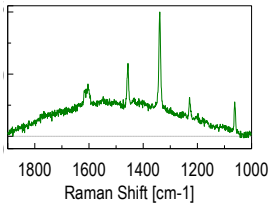	×
1	3.8×10^{4}	5	1	3.8×10^{4}	5	20	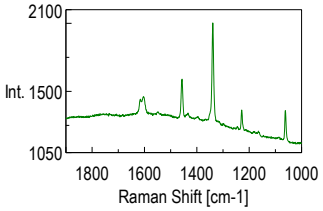	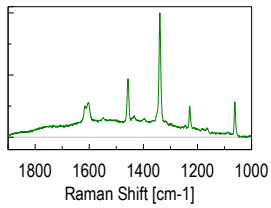	×
0.6	7.4×10^{4}	5	0.6	7.4×10^{4}	5	20	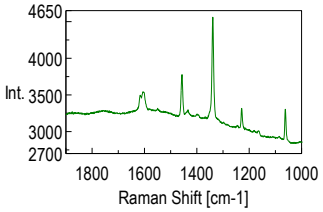	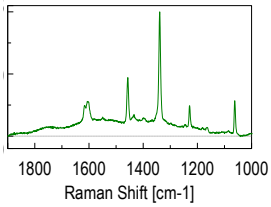	×
0.3	1.5×10^{5}	5	0.3	1.5×10^{5}	5	20	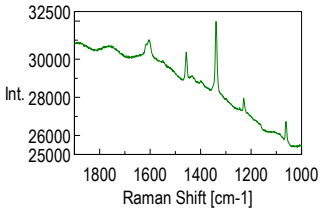	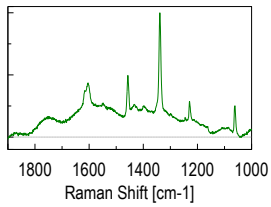	×
0	2.9×10^{5}	300	0	2.9×10^{5}	5	20	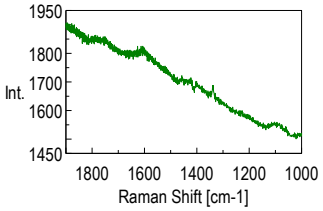	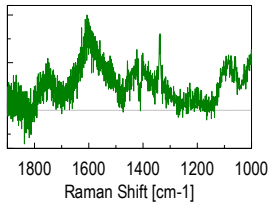	▲

[a] Magnification of objective lens was 100 times.

[b] Optical density (OD) of a neutral density (ND) filter.

[c] Modified spectra were displayed after subtracting linear background and normalizing them for ease of comparing them with each other. Vertical axis exhibits the Raman intensity with arbitrary unit.

[d] ×, ▲, and ○ denote the case when G and D bands were not detected, when it was difficult to judge detection of G and D bands, and when G and D bands were clearly detected, respectively.

Table E3−13. Carbonization and Raman measurement conditions, and the resulting raw and modified Raman spectra after exposing **15** to 532 nm laser.

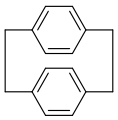

15

Carbonization conditions[a]			Raman measurment conditions[a]				Specra after laser exposure		
OD[b]	Laser energy (W cm^{-2})	Exposure time (s)	OD[b]	Laser energy (W cm^{-2})	Exposure time (s)	Cumulative number	Raw	Modified[c]	G and D bands[d]
1	1.9×10^{4}	60	1	1.9×10^{4}	5	20	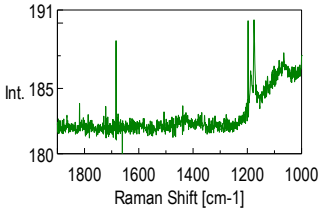	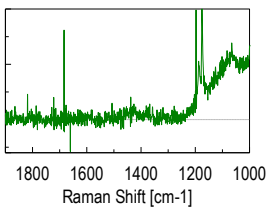	×
0.6	4.8×10^{4}	60	0.6	4.8×10^{4}	5	20	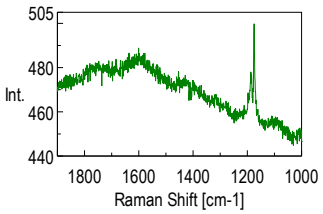	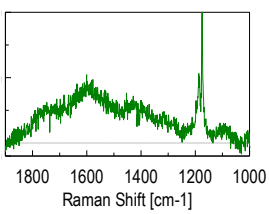	▲
0.3	9.6×10^{4}	60	0.3	9.6×10^{4}	5	20	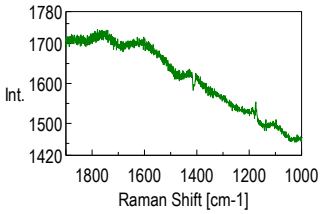	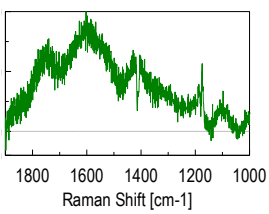	▲
0	1.9×10^{5}	60	0	1.9×10^{5}	5	20	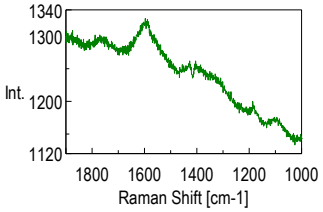	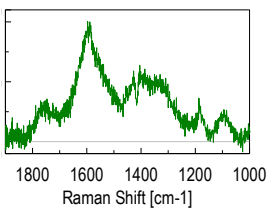	○

[a] Magnification of objective lens was 100 times.
[b] Optical density (OD) of a neutral density (ND) filter.
[c] Modified spectra were displayed after subtracting linear background and normalizing them for ease of comparing them with each other. Vertical axis exhibits the Raman intensity with arbitrary unit.
[d] ×, ▲, and ○ denote the case when G and D bands were not detected, when it was difficult to judge detection of G and D bands, and when G and D bands were clearly detected, respectively.

Table E3−14. Carbonization and Raman measurement conditions, and the resulting raw and modified Raman spectra after exposing **16** to 532 nm laser.

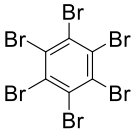

16

Carbonization conditions[a]			Raman measurment conditions[a]				Specra after laser exposure		
OD[b]	Laser energy (W cm^{-2})	Exposure time (s)	OD[b]	Laser energy (W cm^{-2})	Exposure time (s)	Cumulative number	Raw	Modified[c]	G and D bands[d]
1	1.9×10^{4}	60	1	1.9×10^{4}	5	20	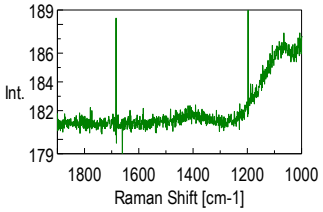	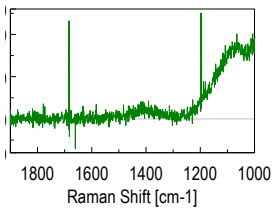	×
0.6	4.9×10^{4}	60	0.6	4.9×10^{4}	5	20	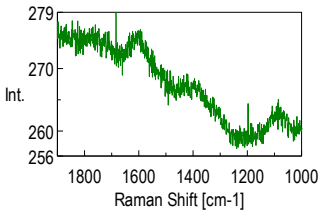	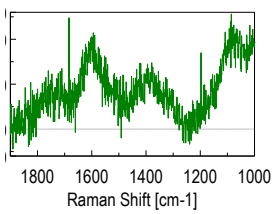	○
0.3	9.7×10^{4}	60	0.3	9.7×10^{4}	5	20	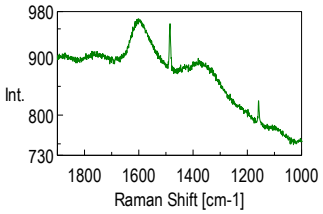	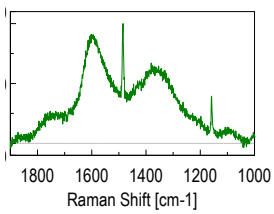	○
0	1.9×10^{5}	60	0	1.9×10^{5}	5	20	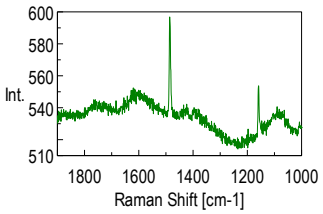	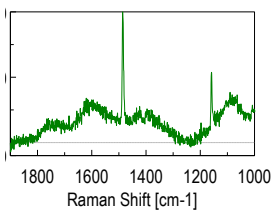	○

[a] Magnification of objective lens was 100 times.

[b] Optical density (OD) of a neutral density (ND) filter.

[c] Modified spectra were displayed after subtracting linear background and normalizing them for ease of comparing them with each other. Vertical axis exhibits the Raman intensity with arbitrary unit.

[d] ×, ▲, and ○ denote the case when G and D bands were not detected, when it was difficult to judge detection of G and D bands, and when G and D bands were clearly detected, respectively.

Table E3−15. Carbonization and Raman measurement conditions, and the resulting raw and modified Raman spectra after exposing **6** to 532 nm laser.

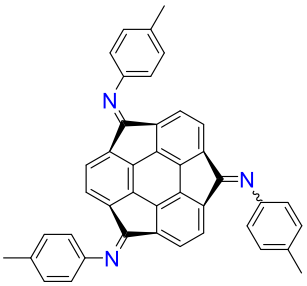

6

Carbonization conditions[a]			Raman measurment conditions[a]				Specra after laser exposure		
OD[b]	Laser energy (W cm^{-2})	Exposure time (s)	OD[b]	Laser energy (W cm^{-2})	Exposure time (s)	Cumulative number	Raw	Modified[c]	G and D bands[d]
3	1.9×10^{2}	100	3	1.9×10^{2}	5	20	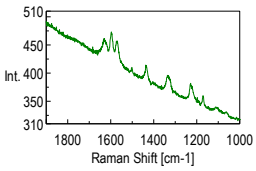	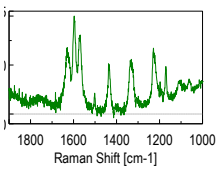	×
2	1.9×10^{3}	60	3	1.9×10^{2}	5	20	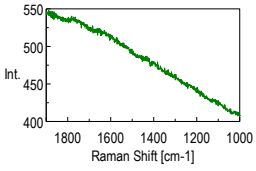	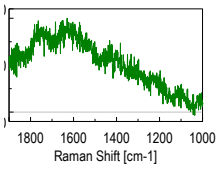	▲
1	1.9×10^{4}	60	3	1.9×10^{2}	5	20	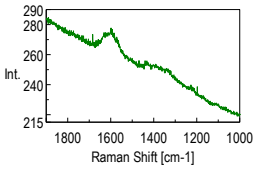	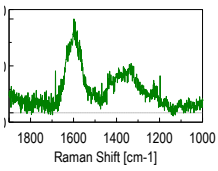	○
0.6	4.9×10^{4}	60	3	1.9×10^{2}	5	20	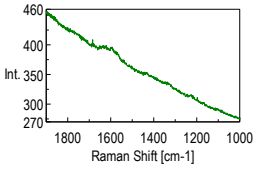	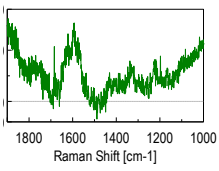	▲
0.3	9.7×10^{4}	60	3	1.9×10^{2}	5	20	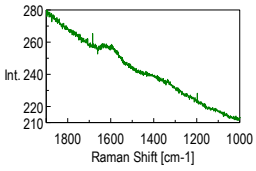	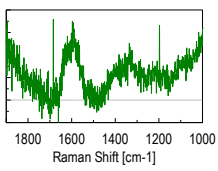	○
0	1.9×10^{5}	60	3	1.9×10^{2}	5	20	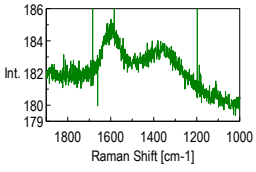	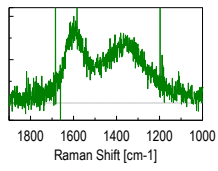	○

[a] Magnification of objective lens was 100 times.

[b] Optical density (OD) of a neutral density (ND) filter.

[c] Modified spectra were displayed after subtracting linear background and normalizing them for ease of comparing them with each other. Vertical axis exhibits the Raman intensity with arbitrary unit.

[d] ×, ▲, and ○ denote the case when G and D bands were not detected, when it was difficult to judge detection of G and D bands, and when G and D bands were clearly detected, respectively.

Table E3−16. Carbonization and Raman measurement conditions, and the resulting raw and modified Raman spectra after exposing **17** to 532 nm laser.

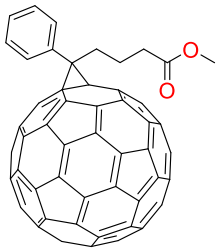

17

Carbonization conditions[a]			Raman measurment conditions[a]				Specra after laser exposure		
OD[b]	Laser energy (W cm^{-2})	Exposure time (s)	OD[b]	Laser energy (W cm^{-2})	Exposure time (s)	Cumulative number	Raw	Modified[c]	G and D bands[d]
2	2.2×10^{2}	300	2	2.2×10^{3}	10	5	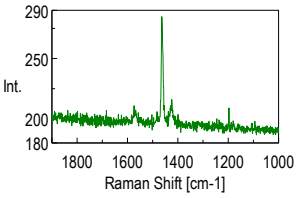	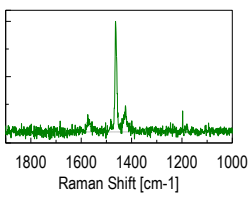	×
1	2.2×10^{3}	300	2	2.2×10^{3}	10	5	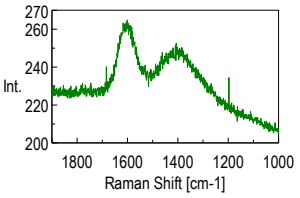	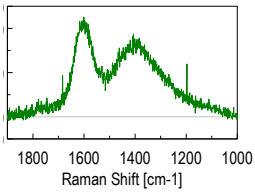	○
0.6	5.4×10^{3}	300	2	2.2×10^{3}	10	5	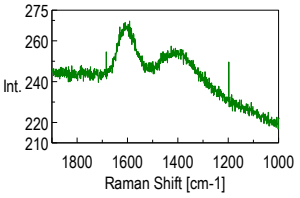	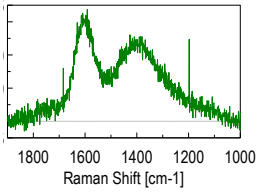	○
0.3	1.0×10^{4}	300	2	2.2×10^{3}	10	5	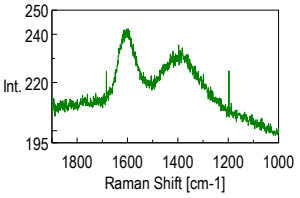	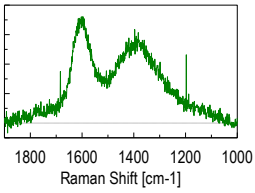	○
0	2.0×10^{4}	300	2	2.2×10^{3}	10	5	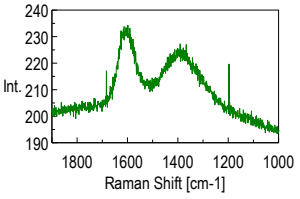	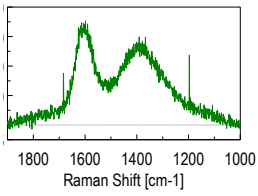	○

[a] Magnification of objective lens was 20 times.

[b] Optical density (OD) of a neutral density (ND) filter.

[c] Modified spectra were displayed after subtracting linear background and normalizing them for ease of comparing them with each other. Vertical axis exhibits the Raman intensity with arbitrary unit.

[d] ×, ▲, and ○ denote the case when G and D bands were not detected, when it was difficult to judge detection of G and D bands, and when G and D bands were clearly detected, respectively.

Density Functional Theory (DFT) Calculation

To estimate the bond dissociation energy (BDE), energy levels of the various species were calculated by density functional theory (DFT) method using the Gaussian 09 program.[12] The vibrational analysis was performed after optimization of the molecule structures. For both the vibrational analysis and structure optimization, the hybrid functional and basis set were B3LYP/6-31G(d,p) and UB3LYP/6-31+G(d,p) for closed-shell and open-shell molecules, respectively.

Calculation of BDEs

Table E3−17 summarizes the sum of electronic and zero-point energies (E) for each species. E of species **n** is denoted by $E_{\mathbf{n}}$. Based on these results, the BDEs of various bonds were calculated by subtracting the E of the species before bond dissociation from that after bond dissociation (see an example in Eq. 1). In the case that two species generate through bond dissociation, the E of the species before bond dissociation was subtracted from the sum of E after bond dissociation (see an example in Eq. 2). The results are also listed in Table E3−17.

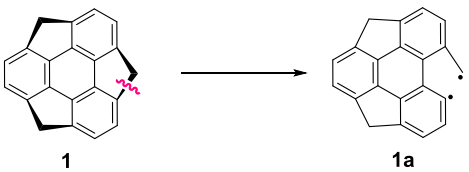

(Eq. 1)

BDE (Ar–CH_2 in **1**) = $E_{\mathbf{1a}} - E_{\mathbf{1}}$

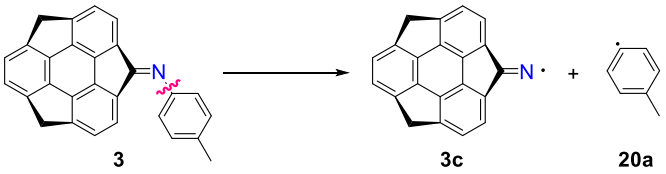

(Eq. 2)

BDE (C=N–Tol in **3**) = $E_{\mathbf{3c}} + E_{\mathbf{20a}} - E_{\mathbf{3}}$

Table E3−17. Sum of electronic and zero-point energies (E) calculated by DFT method. On the right side of the table, calculated BDEs of various bonds are summarized.

Species	E (Hartree per particle)	E (kJ mol^{-1})	Species	E (Hartree per particle)	E (kJ mol^{-1})
1	−807.18871	−2118210	**1a**	−807.141033	−2118085
8	−577.456229	−1515350	**8a**	−577.331545	−1515023
9	−501.250544	−1315373	**9a**	−501.107154	−1314996
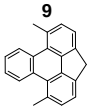 **18**	−809.63291	−2124624	**18a**	−809.522918	−2124335
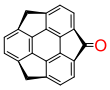 **4**	−881.217211	−2312474	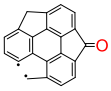 **4a**	−881.175038	−2312364
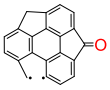 **4b**	−881.172494	−2312357	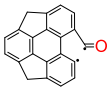 **4c**	−881.160043	−2312324
12	−651.482822	−1709609	**12a**	−651.374542	−1709325
13	−575.279822	−1509639	**13a**	−575.155089	−1509312
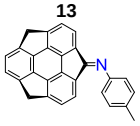 **3**	−1131.599837	−2969524	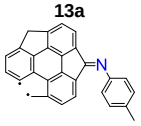 **3a**	−1131.563795	−2969429
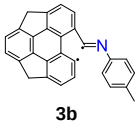 **3b**	−1131.547206	−2969386	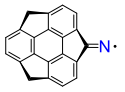 **3c**	−860.71458	−2258672
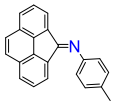 **10**	−901.865229	−2366658	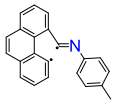 **10a**	−901.768969	−2366406
10b	−630.975893	−1655796	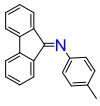 **11**	−825.660342	−2166683
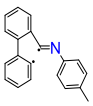 **11a**	−825.542365	−2166373	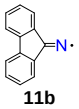 **11b**	−554.770702	−1455819
20a	−270.78567	−710591			

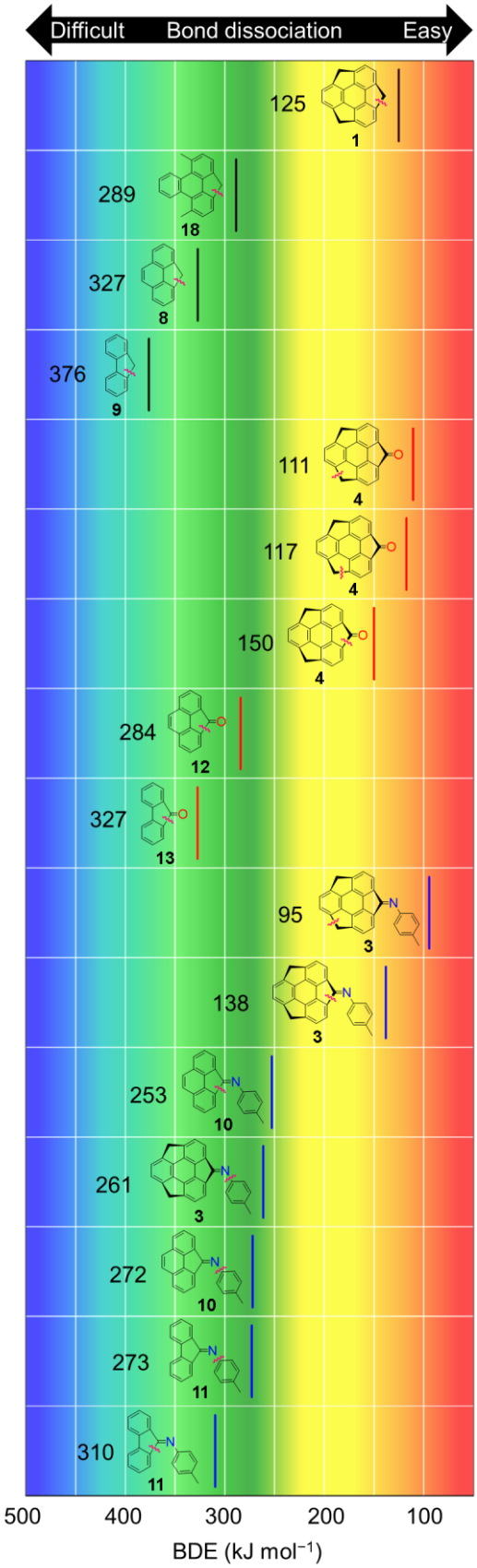

3−5. References and Notes

[1] R. Kostecki, X. Song, K. Kinoshita, *Electrochem. Solid-State Lett.* **2002**, *5*, E29-E31.

[2] a) M. Nakamizo, R. Kammereck, P. L. Walker Jr., *Carbon* **1974**, *12*, 259-267; b) T. Ohnishi, I. Murase, T. Noguchi, M. Hirooka, *Synth. Met.* **1987**, *18*, 497-502; c) M. Endo, K. Hakamada, C. Kim, N. Miyazawa, T. Kasai, *Tanso* **1998**, *183*, 156-161.

[3] a) T. Horaguchi, R. Yamazaki, T. Abe, *Bull. Chem. Soc. Jpn.* **1980**, *53*, 494-497; b) T. Amaya, S. Seki, T. Moriuchi, K. Nakamoto, T. Nakata, H. Sakane, A. Saeki, S. Tagawa, T. Hirao, *J. Am. Chem. Soc.* **2009**, *131*, 408-409; c) L. Giribabu, K. Sudhakar, G. Sabapathi, R. K. Kanaparthi, *J. Photochem. Photobiol., A* **2014**, *284*, 18-26.

[4] a) W. Kaiser, C. G. B. Garrett, *Phys. Rev. Lett.* **1961**, *7*, 229-231; b) Y. H. Pao, P. M. Rentzepis, *J. Chem. Phys.* **1965**, *43*, 1281-1286.

[5] L. T. Scott, M. M. Hashemi, M. S. Bratcher, *J. Am. Chem. Soc.* **1992**, *114*, 1920-1921.

[6] H. Sakurai, T. Daiko, H. Sakane, T. Amaya, T. Hirao, *J. Am. Chem. Soc.* **2005**, *127*, 11580-11581.

[7] a) K. Kuhnke, M. Epple, K. Kern, *Chem. Phys. Lett.* **1998**, *294*, 241-247; b) M. Murata, Y. Morinaka, Y. Murata, O. Yoshikawa, T. Sagawa, S. Yoshikawa, *Chem. Commun.* **2011**, *47*, 7335-7337.

[8] H. Sakurai, T. Daiko, T. Hirao, *Science* **2003**, *301*, 1878.

[9] T. Amaya, M. Hifumi, M. Okada, Y. Shimizu, T. Moriuchi, K. Segawa, Y. Ando, T. Hirao, *J. Org. Chem.* **2011**, *76*, 8049-8052.

[10] W. Dai, R. Srinivasan, J. A. Katzenellenbogen, *J. Org. Chem.* **1989**, *54*, 2204-2208.

[11] G. Sugowdz, P. J. Collin, W. H. F. Sasse, *Tetrahedron Lett.* **1969**, *10*, 3843-3846.

[12] Gaussian 09, Revision C.01, M. J. Frisch, G. W. Trucks, H. B. Schlegel, G. E. Scuseria, M. A. Robb, J. R. Cheeseman, G. Scalmani, V. Barone, B. Mennucci, G. A. Petersson, H. Nakatsuji, M. Caricato, X. Li, H. P. Hratchian, A. F. Izmaylov, J. Bloino, G. Zheng, J. L. Sonnenberg, M. Hada, M. Ehara, K. Toyota, R. Fukuda, J. Hasegawa, M. Ishida, T. Nakajima, Y. Honda, O. Kitao, H. Nakai, T. Vreven, J. A. Montgomery, Jr., J. E. Peralta, F. Ogliaro, M. Bearpark, J. J. Heyd, E. Brothers, K. N. Kudin, V. N. Staroverov, R.

Kobayashi, J. Normand, K. Raghavachari, A. Rendell, J. C. Burant, S. S. Iyengar, J. Tomasi, M. Cossi, N. Rega, J. M. Millam, M. Klene, J. E. Knox, J. B. Cross, V. Bakken, C. Adamo, J. Jaramillo, R. Gomperts, R. E. Stratmann, O. Yazyev, A. J. Austin, R. Cammi, C. Pomelli, J. W. Ochterski, R. L. Martin, K. Morokuma, V. G. Zakrzewski, G. A. Voth, P. Salvador, J. J. Dannenberg, S. Dapprich, A. D. Daniels, Ö. Farkas, J. B. Foresman, J. V. Ortiz, J. Cioslowski, and D. J. Fox, Gaussian, Inc., Wallingford CT, 2009.

Conclusion

In summary, this work focused on the laser-induced carbonization of bowl-shaped molecule sumanene from a viewpoint of studying the important factors affecting the efficiency of carbonization. Chapter 1 described the follow-up of the laser-induced carbonization of sumanene derivatives using the conductivity as a probe to obtain the information about their conductivity and time to reach carbonous products. Through adding the structural analysis to thus-obtained results, Chapters 1and 2 drew the following two conclusions: 1) the increase of the conductivity induced through laser irradiation was based on laser-induced carbonization and 2) NGC was synthesized through the laser-induced carbonization when the nitrogen-containing sumanene derivatives were employed as a starting material. In Chapter 2, moreover, the ORR activity was surveyed for NGCs synthesized through such a method. Chapter 3 dealt with the threshold energy of the laser-induced carbonization of the sumanene skeleton to investigate its susceptibility through comparing it to that of other compounds having similar chemical structures. Such investigation is expected to lead to evaluation of dependence of susceptibility to laser-induced carbonization on starting materials. These findings are considered to contribute toward development of laser-induced-carbonization-based chemistry as well as chemistry of bowl-shaped molecule sumanene.

List of Publications

1. Nitrogen-doped Graphitic Carbon Synthesized by Laser Annealing of Sumanenemonoone Imine as a Bowl-shaped π-Conjugated Molecule
   Yuhi Inada, Toru Amaya, Yasutomo Shimizu, Akinori Saeki, Takeo Otsuka, Ryotaro Tsuji, Shu Seki, and Toshikazu Hirao
   Chem. Asian J. **2013**, *8*, 2569-2574.

2. Sumanenemonoone Imines Bridged by Redox-active π-Conjugated Unit: Synthesis, Stepwise Coordination to Palladium (II), and Laser-induced Formation of Nitrogen-doped Graphitic Carbon
   Toru Amaya, **Yuhi Inada**, Yasutomo Shimizu, Akinori Saeki, Ryotaro Tsuji, Shu Seki, and Toshikazu Hirao
   Chem. Asian J. **2014**, *9*, 2568-2575.

3. Laser-induced Carbonization of Sumanene Derivatives: Exposure-time Dependence of Time-resolved Microwave Conductivity
   Yuhi Inada, Toru Amaya, Akinori Saeki, Shu Seki, and Toshikazu Hirao
   Bull. Chem. Soc. Jpn. **2015**, *88*, 330-332.

4. Investigation of Threshold in Laser-induced Carbonization of Sumanene Derivatives through *In situ* Observation Utilizing a Raman Spectroscope
   Yuhi Inada, Toru Amaya, and Toshikazu Hirao
   RSC Adv. **2015**, *5*, 18523-18530.

5. Oxygen Reduction Reaction Activity of Nitrogen-doped Graphitic Carbon Synthesized through Laser-induced Carbonization of Sumanene Derivative
   Yuhi Inada, Toru Amaya, Shohei Morohoshi, Junji Nakamura, and Toshikazu Hirao
   In preparation.

List of Supplementary Publications

S1. Giant Organic Single-crystals of a Thiophene/phenylene Co-oligomer toward Device Applications
Yuhi Inada, Takeshi Yamao, Mari Inada, Toshiaki. Itami, and Shu Hotta
Synth. Met. **2011**, *161*, 1869-1877.
(This paper was selected as a cover picture.)

S2. Gold Nanoparticles Catalyst with Redox-active Poly(aniline sulfonic acid): Application in Aerobic Dehydrogenative Oxidation of Cyclic Amines in Aqueous Solution
Toru Amaya, Tsubasa Ito, **Yuhi Inada**, Daisuke Saio, and Toshikazu Hirao
Tetrahedron Lett. **2012**, *53*, 6144-6147.

S3. Synthesis of Self-doped Conducting Polyaniline Bearing Phosphonic Acid Monoester
Toru Amaya, Yasushi Abe, **Yuhi Inada**, and Toshikazu Hirao
Synth. Met. **2014**, *195*, 137-140.

S4. Synthesis of Self-doped Conducting Polyaniline Bearing Phosphonic Acid
Toru Amaya, Yasushi Abe, **Yuhi Inada**, and Toshikazu Hirao
Tetrahedron Lett. **2014**, *55*, 3976-3978.

S5. Characterization of Self-doped Conducting Polyanilines Bearing Phosphonic Acid and Phosphonic Acid Monoester
Yasushi Abe, Toru Amaya, **Yuhi Inada**, and Toshikazu Hirao
Synth. Met. **2014**, *197*, 240-245.

S6. Preparation of Polyaniline-Pt Nanoparticles via Ligand Exchange from Starch-Pt Nanoparticles
Tadayuki Isaji, Toru Amaya, **Yuhi Inada**, Masashi Abe, and Toshikazu Hirao
Bull. Chem. Soc. Jpn. **2014**, *87*, 1130-1132.

Acknowledgement

The author would like to express his sincerest acknowledgment to Professor Dr. Toshikazu Hirao, Department of Applied Chemistry, Graduate School of Engineering, Osaka University for his continuous guideline throughout this work and fruitful discussions.

The author would like to deeply express his appreciation to Professor Dr. Hidehiro Sakurai and Professor Satoshi Minakata, Department of Applied Chemistry, Graduate School of Engineering, Osaka University for reviewing this thesis and helpful comments.

The author would like to express his appreciation and gratitude to Dr. Toru Amaya, Department of Applied Chemistry, Graduate School of Engineering, Osaka University for his continuous guidance throughout these works, so many helpful suggestions, fruitful discussions, and hearty encouragement.

The author would like to express his special thanks to Dr. Toshiyuki Moriuchi, Department of Applied Chemistry, Graduate School of Engineering, Osaka University for his so many helpful advice and hearty encouragement.

The author would like to appreciate Professor Dr. Shuhei Seki and Dr. Akinori Saeki, Department of Applied Chemistry, Graduate School of Engineering, Osaka University for the TRMC measurements.

The author would like to be grateful to Professor Dr. Nobuhito Imanaka and Dr. Toshiyuki Masui, Department of Applied Chemistry, Graduate School of Engineering, Osaka University for the Raman measurements.

The author would like to give recognition to the members of the Comprehensive Analysis Center, ISIR, Osaka University for the GI-XRD measurements.

The author would like to feel grateful about Dr. Kinya Katano, Office for University-Industry Collaboration, Osaka University for the XPS measurements.

The author would like to acknowledge for Professor Dr. Junji Nakamura and Mr. Shohei Morohoshi, Graduate School of Pure and Applied Sciences, University of Tsukuba for the ORR measurements.

The author would like to appreciate very much to all members of Professor Dr. Toshikazu Hirao's group for their hearty encouragement, supports, and friendship.

The author would be grateful for financial supports by Grants for Excellent Graduate Schools of Osaka University and Japan Society for the Promotion of Science.

Finally the author would like to express his special thanks to his parents and family for their constant encouragement, supports, and understanding on this work.

Yuhi Inada